Atmos. Chem. Phys., 7, 3285–3308, 2007
www.atmos-chem-phys.net/7/3285/2007/

Atmospheric Chemistry and Physics

Contribution of mixing to upward transport across the tropical tropopause layer (TTL)

P. Konopka[1], G. Günther[1], R. Müller[1], F. H. S. dos Santos[1], C. Schiller[1], F. Ravegnani[2], A. Ulanovsky[3], H. Schlager[4], C. M. Volk[5], S. Viciani[6], L. L. Pan[7], D.-S. McKenna[7], and M. Riese[1]

[1]Forschungszentrum Jülich (ICG-1: Stratosphäre), Germany
[2]CNR-ISAC, Bologna, Italy
[3]CAO, Dolgoprudny, Russia
[4]Institut für Physik der Atmosphäre, DLR Oberpfaffenhofen, Germany
[5]Institut für Meteorologie und Geophysik, Universität Frankfurt, Germany
[6]INOA, Firenze, Italy
[7]National Center for Atmospheric Research, Boulder, CO, USA

Received: 25 October 2006 – Published in Atmos. Chem. Phys. Discuss.: 28 November 2006
Revised: 23 March 2007 – Accepted: 12 June 2007 – Published: 26 June 2007

Abstract. During the second part of the TROCCINOX campaign that took place in Brazil in early 2005, chemical species were measured on-board the high-altitude research aircraft Geophysica (ozone, water vapor, NO, NO_y, CH_4 and CO) in the altitude range up to 20 km (or up to 450 K potential temperature), i.e. spanning the entire TTL region roughly extending between 350 and 420 K.

Here, analysis of transport across the TTL is performed using a new version of the Chemical Lagrangian Model of the Stratosphere (CLaMS). In this new version, the stratospheric model has been extended to the earth surface. Above the tropopause, the isentropic and cross-isentropic advection in CLaMS is driven by meteorological analysis winds and heating/cooling rates derived from a radiation calculation. Below the tropopause, the model smoothly transforms from the isentropic to the hybrid-pressure coordinate and, in this way, takes into account the effect of large-scale convective transport as implemented in the vertical wind of the meteorological analysis. As in previous CLaMS simulations, the irreversible transport, i.e. mixing, is controlled by the local horizontal strain and vertical shear rates.

Stratospheric and tropospheric signatures in the TTL can be seen both in the observations and in the model. The composition of air above ≈350 K is mainly controlled by mixing on a time scale of weeks or even months. Based on CLaMS transport studies where mixing can be completely switched off, we deduce that vertical mixing, mainly driven by the vertical shear in the tropical flanks of the subtropical jets and, to some extent, in the the outflow regions of the large-scale convection, offers an explanation for the upward transport of trace species from the main convective outflow at around 350 K up to the tropical tropopause around 380 K.

Correspondence to: P. Konopka
(p.konopka@fz-juelich.de)

1 Introduction

The composition of the air entering the stratosphere is mainly determined by the transport processes within the tropical tropopause layer (TTL) (Atticks and Robinson, 1983) coupling the Hadley circulation in the tropical troposphere with the much slower, Brewer-Dobson circulation in the stratosphere. Whereas the former is dominated by convective processes, the latter is driven mainly by radiation and extratropical wave drag (Holton et al., 1995).

The lowest boundary of the TTL, around θ =350 K isentropic surface (see Fig. 1), can be defined by the level of the main convective outflow (Gettelman and de Forster, 2002; Folkins and Martin, 2005). The upper limit of the TTL is expected to be above the cold point tropopause at around 380 K but below ≈420 K, marking the highest level of the observed deepest convection events (Kelly et al., 1993; Sherwood and Dessler, 2001).

Laterally, the TTL is confined by the subtropical jets (STJ), which vary seasonally both in their intensity and meridional position (yellow ellipses in Fig. 1), with a strong, equatorwards shifted jet in the winter hemisphere and a weak, meandering, polewards shifted STJ in the summer hemisphere. Following the concept of effective diffusivity, Haynes and Shuckburgh (2000) showed that a strong

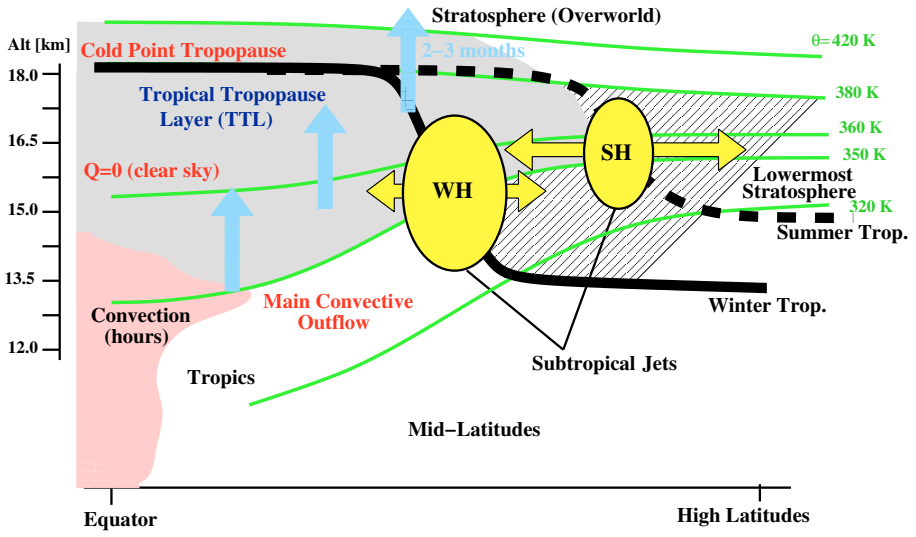

Fig. 1. Schematic of transport processes connecting the tropical tropopause layer (TTL, dark gray) with the stratosphere. Whereas the quasi-isentropic transport processes across the subtropical jets (STJs, yellow) dominate the exchange between the TTL and the lowermost stratosphere (dashed), the vertical transport across the TTL lifts tropospheric air into the stratospheric overworld. This transport path starts approximately at the main convective outflow level around $\theta \approx 350$ K and, following the blue arrows, crosses the level of zero clear sky radiative heating ($Q=0$) around 360 K, and finally reaches the lower stratosphere above the cold point tropopause at around 380 K. Both quasi-isentropic and vertical transport depend on season, with different strengths and positions of the STJs in the winter (WH) and summer hemispheres (SH).

STJ forms an effective transport barrier for the meridional, quasi-isentropic transport between the TTL and midlatitudes with the highest permeability during monsoon circulations, mainly in the Northern Hemisphere, when a strong upper-level anticyclone over south-east Asia disrupts the zonal symmetry of the STJ. Furthermore, Haynes and Shuckburgh (2000) concluded that STJ in the southern summer hemisphere is generally a stronger transport barrier than in the Northern Hemisphere during the same season.

Because deep convection events transporting air directly into the stratosphere seem to be too rare to supply the Brewer-Dobson circulation with sufficient mass (Gettelman et al., 2002), the question arises of other possible physical mechanisms for the troposphere-to-stratosphere transport, TST (in the following, the reverse transport is abbreviated as STT), that lifts air masses from the main convective outflow around 350 K across the TTL into the lower stratosphere. The typical time scales for this transport, as derived from the upward propagation of the seasonal cycle of CO_2 arising in the planetary boundary layer, vary between 2 and 3 months for the upward transport from $\theta=350$ K to 390 and 420 K, respectively (Andrews et al., 1999).

It is generally believed that the radiative heating effectively lifts air masses within the TTL above the $Q=0$ level where the background clear sky heating rate changes from a net cooling below to a net heating above. This transition level was generally found at an almost constant value of $\theta=360$ K ($\approx$15 km) (Gettelman et al., 2004). The transition from radiative cooling to radiative heating is driven by the combination of a rapid decrease in water vapor mixing ratios (longwave cooling is negligible above 360 K), suppressed longwave emission from CO_2 and ozone due to extremely cold temperatures and an increase of shortwave heating above 360 K owing to enhanced ozone mixing ratios.

Although, this explanation is widely subscribed to, there remain aspects of TST that are not adequately addressed, for instance: How do air parcels overcome the vertical gap between the main convective outflow around 350 K and the level with significant heating rates? Normally, air parcels within the outflow region of the convective towers sink due to radiative cooling rather than ascend into the stratosphere. Clouds in the TTL tend to increase the potential temperature where $Q=0$ occurs due to suppressed longwave heating from the earth's surface of the air masses above clouds (Doherty et al., 1984; Gettelman et al., 2004). Consequently, clouds increase the gap between the convective outflow and radiation driven transport by up to $\approx$25 K. Recently, Corti et al. (2006) proposed a new radiation-based mechanism showing that lofting due to heating within thin cirrus clouds has the potential to overcome this gap but there is still neither experimental evidence nor 3-D transport studies driven by realistic winds and cirrus cloud distributions which would support this theory.

Here, we propose an alternative, non-advective, mechanism for TST across the TTL mainly based on mixing in this region as diagnosed by the Chemical Lagrangian Model of

the Stratosphere (CLaMS) (McKenna et al., 2002; Konopka et al., 2004). We show that the concept of deformation-induced mixing driven by large-scale meteorological winds as implemented in CLaMS identifies the TTL as a region with enhanced horizontal and vertical gradients in the horizontal wind, i.e. as a region with increased horizontal strain and vertical shear rates, mainly occurring in the vicinity of the STJs, preferably on their tropical sides but also in the tropics in the outflow of large-scale convective systems. Furthermore, we also show that these high deformation rates have the potential to enhance diffusive fluxes, in particular those of the trace gases with horizontal and/or vertical gradients, and that such diffusive fluxes may contribute to the transport across the tropopause.

The importance of the STJs as mixing barriers for horizontal transport across the tropopause separating the TTL from the lowermost stratosphere was recently discussed by d'Ovidio et al. (2007)[1]. Using the concept of the (Lyapunov) effective diffusivity, they diagnosed an enhanced isentropic mixing at the θ=350 K level, mainly within the tropics confined by the STJs and with the highest values on the tropical side of these jets but with a clear minimum at their centers.

Observations of ozone filaments around the STJs formed by breaking Rossby waves (Bradshaw et al., 2002a,b) or measurements of increased turbulence caused by shear-induced gravity waves (Pavelin and Whiteway, 2002) also indicate enhanced mixing in these regions. Furthermore, the reverse-domain-filling technique (RDF) with Lagrangian mixing (Legras et al., 2005) has had some success in reconstructing tracer structures that are not resolved by conventional CTMs and has demonstrated that enhanced mixing correlates with high Lyapunov exponents measuring the deformations in the flow. This property also characterizes the CLaMS parameterization of mixing, e.g. strongly enhanced mixing in CLaMS can be found in the flanks of the subtropical jet (Pan et al., 2006).

Generally, there are two ways how the tropospheric air within the TTL can enter the stratosphere. The most dominant part (about 95% of the mass, Levine et al., 2007) crosses the STJs quasi-isentropically, mainly across the weak summer jets and reaches the lowermost stratosphere, i.e. the descending branch of the Brewer-Dobson circulation, whereas only a relatively small part (<5%) enters the stratosphere (overworld). In this paper, we propose that, in addition to the isentropic mixing across the STJs, the deformation-driven, irreversible vertical transport in CLaMS offers an alternative mechanism for the upward transport of trace species across the TTL.

The paper is organized as follows. In the next section we describe the newly improved version of CLaMS. In this new version, the stratospheric CTM is extended through a hybrid coordinate to the surface, incorporating the entire troposphere. To validate this new version, we use in situ observations on-board the high-altitude Russian aircraft Geophysica during the TROCCINOX (Tropical Convection, Cirrus and Nitrogen Oxides Experiment) campaign in early 2005 in Brazil that is briefly described in Sect. 3. In particular, to validate both STT and TST, in Sects. 4 and 5, respectively, we compare the simulated tracer distributions with data obtained during two long-range flights penetrating the TTL. In Sect. 6, we discuss the contribution of mixing to the transport across the TTL and, finally, conclusions are drawn in Sect. 7.

2 Model description: CLaMS with stratosphere and troposphere

To resolve transport processes in the troposphere, in particular within the TTL, the vertical coordinate of CLaMS was extended from the potential temperature θ, to a hybrid pressure-potential temperature coordinate ζ (Mahowald et al., 2002). In this section, we describe some details of this extension mainly focusing on implications for the vertical transport, in particular in regions affected by convection and by the STJ.

2.1 Hybrid vertical coordinate

Following the procedure proposed by Mahowald et al. (2002), we generalize the potential temperature, θ, to a hybrid coordinate, ζ, that below a certain pressure level, p_r, approximating the tropopause (i.e. for pressure values $p > p_r$) smoothly transforms from isentropic to pressure coordinates:

$$\zeta(p) = f(\eta)\theta(p, T(p)), \quad \eta = \frac{p}{p_0} \tag{1}$$

with

$$f(\eta) = \begin{cases} \sin\left(\frac{\pi}{2}\frac{1-\eta}{1-\eta_r}\right) & \eta > \eta_r \\ 1 & \eta \le \eta_r, \quad \eta_r = \frac{p_r}{p_0} \end{cases} \tag{2}$$

and $\theta = T(p_0/p)^\kappa$, κ=0.286. Here, T denotes the temperature, p_0=1013 hPa is the constant surface pressure at sea level and p_r=100 hPa. This pressure level roughly corresponds to the pressure at the tropical tropopause.

The ζ-coordinate is illustrated in the left panel of Fig. 2. Here, as an example, the isolines of the zonally averaged pressure p (blue) and potential temperature θ (orange) were calculated for one particular ECMWF data set (1 January 2004, 12:00 UT) and plotted as a function of latitude and the hybrid coordinate ζ. Above approximately ζ=380 K, the θ-isolines and the ζ-coordinates are the same, whereas the $p-$isolines cross the $\zeta-$levels. In contrast, below about ζ=300 K, the p and ζ levels tend to become parallel to each other (even if the units of ζ are Kelvin), whereas the isentropes cross these lines. The ζ=0 level exactly corresponds to $p=p_0$. The black region is confined by the ζ=0 level

[1] d'Ovidio, F., Legras, B., and Shuckburgh, E.: Local diagnostic of mixing and barrier modulation at the tropopause, J. Atmos. Sci., submitted, 2007.

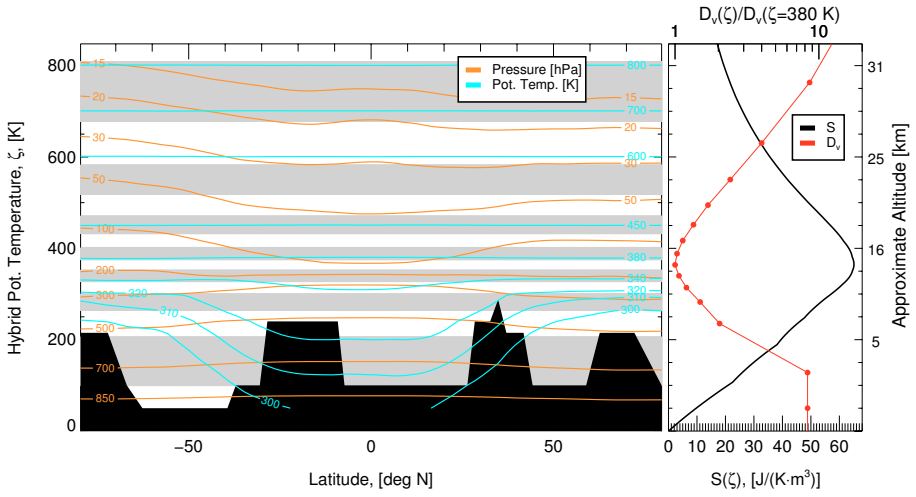

Fig. 2. CLaMS hybrid vertical coordinate ζ. Left: Entropy-preserving CLaMS layers $\Delta\zeta$ colored alternating gray and white are overlaid by the isolines of zonally averaged pressure p (orange) and potential temperature θ (blue) (as an example derived for one ECMWF data set at 1 January 2004, 12:00 UT). Right: Entropy profile $S(\zeta)$ (black) derived from Eq. (3) for the US standard atmosphere. The condition ΔS=const in every layer $\Delta\zeta$ was used to generate CLaMS layers. The red bold dots denote the relative vertical diffusivity $D_v(\zeta)/D_v(\zeta{=}380\,\mathrm{K})$ calculated for one mixing event between two adjacent air parcels.

and the highest values of the orography within each latitude bin (e.g. the highest point corresponds to the elevation of the summit of Himalayas).

2.2 Entropy-preserving distribution of air parcels

Unlike Eulerian CTMs, CLaMS considers an ensemble of air parcels on a time-dependent irregular grid (McKenna et al., 2002; Konopka et al., 2004, 2005). The initial positions of the air parcels have to be specified both in the horizontal and vertical. For a given horizontal resolution, i.e. the mean horizontal separation r_0 between adjacent air parcels, their mean vertical separation is, at first, a free parameter.

The layerwise mixing concept in CLaMS (i.e. the deformation-induced mixing is applied layerwise, with each layer containing approximately the same number of air parcels) requires that a grid of vertical layers, each with the thickness $\Delta\zeta$, has to be defined. Generally, $\Delta\zeta$ depends on ζ. In every layer, the air parcels are approximately uniformly distributed over the layer thickness $\Delta\zeta$ and, consequently, the mean vertical separation between the air parcels is given by $\Delta\zeta/2$ or, in geometric space, by $\Delta z/2$ where z denotes the geometric altitude. The dependence of $\Delta\zeta$ on ζ is motivated by the following ideas.

The ratio between r_0 and $\Delta z/2$ in a given layer $\Delta\zeta$, the so-called aspect ratio α, controls not only the consistency between the horizontal and vertical resolution of the model (in the sense that the tracer variability is resolved, both horizontally and vertically, to the same degree) but, in addition, α also controls the horizontal and vertical diffusivities of the air parcels involved in a mixing event. Because these diffusivities are proportional to r_0^2 and $\Delta z^2/4$, respectively (Konopka et al., 2004, this can also be derived from the dimensional analysis of the diffusion equation for the mixing ratio μ, $\dot{\mu}{=}D\nabla^2\mu$, $D{\sim}L^2/T$, L, T-typical length and time scales), an appropriate choice of α also guarantees that the ratio between the horizontal and vertical diffusivity is correctly described.

From observations and theoretical estimates, Haynes and Anglade (1997) concluded that α=250 is a good choice for the lower stratosphere. Using this value and the potential temperature as the vertical coordinate, CLaMS simulations, mainly in the lower stratosphere, successfully reproduced the observed small-scale structures as filaments, vortex remnants or tracer gradients across the vortex edge (Konopka et al., 2003, 2004; Grooß et al., 2005).

Because the assumption of α=const cannot be applied for the troposphere (where much stronger vertical mixing is expected than in the lower stratosphere) and for the middle and upper stratosphere (where only an increase of the vertical diffusivity with altitude can explain the observed profiles in terms of the 1-D age studies (Ehhalt et al., 2004)), we need an additional criterion to determine the vertical spacing $\Delta\zeta$ of the vertical layers, in particular if the CLaMS domain extends from the earth's surface up to the stratopause.

Here, as a criterion for determining the dependence of $\Delta\zeta$ on ζ, we propose to assume that the volume of each air parcel contains the same amount of entropy S (Holton, 1992):

$$S \sim c_p n \ln \frac{\theta}{\theta_0} \tag{3}$$

with specific heat c_p, air density n, potential temperature θ

and the reference potential temperature θ_0 (i.e. entropy understood as an extensive quantity, so we have to multiply the entropy density $s=c_p \ln(\theta/\theta_0)$ by the air density n). Using θ and n profiles of the US standard atmosphere, $S(\zeta)$ calculated from Eq. (3) is plotted in the right panel of Fig. 2 (black) showing a clear maximum around 15 km. This is because θ increases while n decreases with altitude (or with ζ) and, consequently, $S(\zeta)$, which is proportional to $n \ln\theta$, has a maximum.

Thus, in the new version of CLaMS, the vertical grid of layers is defined in the following way (see left panel of Fig. 2 where such layers are colored alternating gray and white). First, for a given horizonal resolution r_0 and aspect ratio α (here α=250), a layer in the lower stratosphere with a geometric thickness $\Delta z=\alpha r_0$ is calculated (here around ζ=380 K) and then transformed first to Δp using the US standard atmosphere and then to $\Delta\zeta$ by applying Eq. (1).

By assuming that the total amount of entropy in this layer, ΔS, should be the same for all layers (i.e. ΔS=const), we define the thickness $\Delta\zeta$ of all other layers. Thus, by taking into account the entropy S calculated for the U.S. standard atmosphere, the entropy-preserving layers with variable vertical spacing are created. An example is shown in Fig. 2 where r_0=200 km was specified.

In atmospheric models, the vertical resolution is mostly kept constant over the model domain and often chosen independently of the horizontal resolution. Although there can be no mathematical proof of our proposed method to determine a vertical spacing that varies with altitude, there are some arguments which support the idea of the entropy-preserving layers.

First, the relative vertical diffusivity of one mixing event estimated from $D_v(\zeta)/D_v$ (ζ=380 K)$\approx\Delta z^2(\zeta)/\Delta z^2(\zeta$=380 K) and shown on the right side of Fig. 2 (red line) increases with distance from the ζ=380 level by a factor of 10 around 30 km. This is in qualitative agreement with the expected relative increase of the vertical diffusivity as derived from the investigations of the age of air and of (1-D) eddy diffusion coefficients (Ehhalt et al., 2004). Note that the vertical grid with the thinnest layer around the tropical tropopause also implies the lowest vertical diffusivity per mixing event in this region.

Another argument is based on the maximum of entropy S near the tropopause (black line in the right panel of Fig. 2, see also Emanuel, 2003, and references therein). If questions of mixing, i.e. of entropy production, are discussed, a higher resolution of the mixing-dominated parts of the atmosphere is required. The entropy-based measure of mixing at the tropopause was recently discussed by Patmore and Toumi (2006) showing that half of the entropy produced by mixing can be attributed to subtropical "Rossby-driven" tropopause folding events and that the remaining part can be associated with tropical convective mixing and shear-induced mixing at the STJs.

Thus, high entropy production occurs near the tropopause, i.e. in a region where the entropy itself reaches its highest values. We conclude from such arguments that, if mixing in a discrete model like CLaMS is represented by creating new air parcels and if the entropy is equally resolved over the whole model domain, than each mixing event represents approximately the same value of the mixing-induced entropy production.

2.3 Hybrid vertical velocity

An important advantage of the $\zeta-$coordinate is that it allows the vertical velocities in the troposphere as implemented in the meteorological data (that is $\dot{p}=\omega$, ω-vertical velocity in the p-coordinate), in particular the large-scale, convection-driven transport in the tropics (i.e. convection understood as a convection-induced bulk or mean vertical velocity averaged within a grid box of the meteorological model) to be coupled with the radiation-driven vertical velocities in the stratosphere ($\dot{\theta}=Q$, Q-heating rate).

Thus, as in the previous version of CLaMS, the isentropic and cross-isentropic advection above the tropopause is driven here by ECMWF winds and heating/cooling rates derived from the Morcrette scheme under clear sky conditions (Morcrette, 1991; Zhong and Haigh, 1995).

Below the tropopause, where the $\zeta-$coordinate behaves like a pressure coordinate, the ECMWF ω-velocity is used, which, within the ECMWF model, is derived from the continuity equation (Simmons et al., 1999). Strong updrafts due to enhanced values of ω were found in the ECMWF analysis in regions where large-scale convection such as that organized in the mesoscale convective systems (MCS) occurred (e.g. Hegglin et al., 2004). According to Mahowald et al. (2002), the time derivative of ζ follows from its definition (Eq. 1):

$$\dot{\zeta} = \frac{d\zeta}{dt} = \dot{f}\theta + f\dot{\theta} \tag{4}$$

with

$$\dot{f} = \begin{cases} \frac{\pi}{2}\frac{\dot{\eta}}{\eta_r - 1}\cos\left(\frac{\pi}{2}\frac{1-\eta}{1-\eta_r}\right) & \eta > \eta_r \\ 0 & \eta \le \eta_r \end{cases} \tag{5}$$

and $\dot{\eta} = \dot{p}/p_0$.

Generally, the first term in Eq. (4) dominates the second in convective regions. When $\dot{p}$ is negligible (e.g. away from convective regions in the tropics), Eq. (4) reduces to $\dot{\zeta}=f\dot{\theta}$. Thus, for p_r=100 hPa (as used here), the factor f decreases from 1, to 0.97, and 0.9 at p=100, 200 and 300 hPa, respectively, guaranteeing that radiation, i.e. $\dot{\theta}$, dominates the vertical velocities in the TTL in regions not affected by convection.

Below the tropopause, the enhanced values of $\dot{\zeta}$ are dominated by large-scale convection. To illustrate this, in Fig. 3 we give an example of diagnosing fast vertical transport using 5-days backward trajectories starting from the

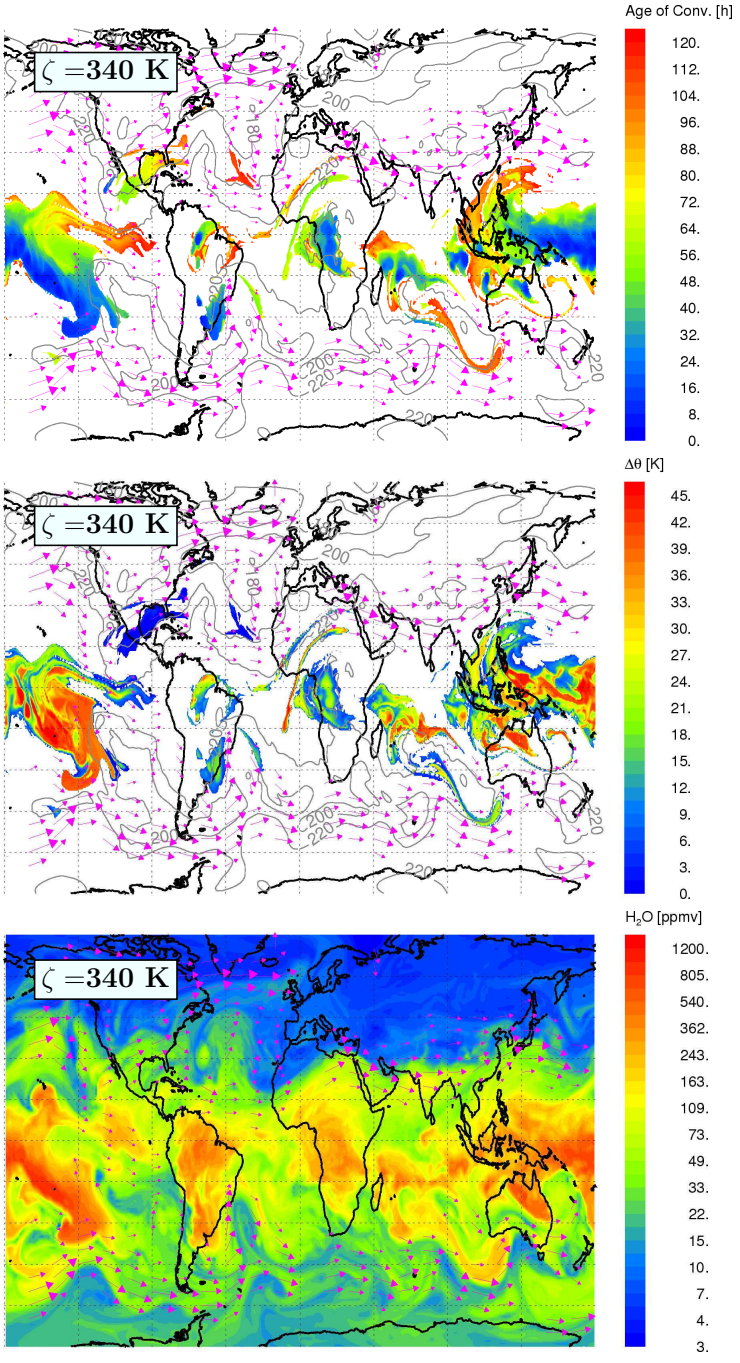

Fig. 3. Age of convection (top), $\Delta\theta$ experienced along the trajectories (middle) and the ECMWF water vapor distribution at ζ=340 K (bottom). The age of convection is derived from the 5-day backward trajectories starting at this level on 8 February 2005, 12:00 UT, and is defined as the time lag between the initialization time and the time when the trajectory descended below p_c=300 hPa. $\Delta\theta$ denotes the increase of the potential temperature experienced by air parcels along these trajectories (positive values mean ascent with increasing time). Overlaid are wind vectors (pink) plotted for wind velocities higher than 20 m/s and indicating the positions of STJs. The gray lines denote the pressure isolines.

ζ=340 K surface (i.e. $p\approx$180 . . . 220 hPa) on 8 February 2005, 12:00 UT (there is no preference for this apart from the fact that it coincides with a Geophysica flight that will be discussed below). The wind vectors (pink) highlight the position of the STJs, with higher values in the winter Northern Hemisphere ($u>$60 m/s) than in the summer Southern Hemisphere.

To identify regions where strong updraft occurred in the last 120 h, the elapsed time until a (backward) trajectory descended below p_c=300 hPa is shown in the top panel of Fig. 3. In the middle panel of Fig. 3 we consider the change of the potential temperature, $\Delta\theta$, experienced by the air parcel along the trajectories (positive values mean ascent with increasing time).

We assume that if $\Delta\theta$ values higher than 20 K occur on a time scale of the order 24 h, the corresponding regions can be identified as regions affected by the large-scale convection. In the following, we denote this elapsed time as the age of convection. Thus, between Indonesia and the south-eastern Pacific a strong, large-scale updraft in the last 24 h was found in a baroclinic weather system while over Brazil, Central Africa and Madagascar regions with a more localized convection were identified.

Now, we compare these signatures of large-scale upward transport with the analyzed ECMWF specific humidity (H_2O) distribution (bottom panel of Fig. 3). The ECMWF H_2O distribution is a result of a 4-D variational analysis (4D-Var) combining the radiosonde and satellite observations with transport calculations constrained by the six-hourly analysis of wind and temperature (Simmons et al., 1999). The vertical transport of H_2O in the ECMWF model is driven not only by the ω-velocity but, in addition, by sub-grid convective transport based on the Tiedtke (1989) parameterization. Furthermore, condensation and evaporation processes convert water between the gaseous, liquid and solid states.

Thus, the spatial distribution of the enhanced H_2O values in the upper troposphere can be understood as a proxy for the fresh upward transport. In particular, between Indonesia and the south-eastern Pacific, this distribution correlates fairly well with the large-scale, upward transport derived from pure trajectory calculations. A significantly increased density of high clouds in this region was also observed by the GOES satellite (not shown) indicating that large-scale convection in connection with an ascent associated with latent heat release is responsible for these patterns.

Finally, to illustrate the typical meridional and vertical distribution of $\dot{\zeta}$, zonally and monthly averaged values calculated for March, June, September and December 2003 are shown in Fig. 4. The vertical axis is rescaled by the use of the entropy function $S(\zeta)$ (see Fig. 2, right panel), so the entropy density does not change along the vertical axis. In this way, the tropopause region is expanded relative to the troposphere and to the stratosphere. The gray contour defined by $\dot{\zeta}$=0 separates the regions with positive (ascent) from regions with negative values of $\dot{\zeta}$ (descent). The position of the tropopause (blue lines) is inferred from the |PV|=2–4 isolines in the extratropics and θ=380 K in the tropics. The p- and θ-isolines (black and pink) define the physical coordinates whereas $\zeta=\theta$ is valid only in the stratosphere.

Thus, in the tropics, above θ=360 K, the radiatively driven ascent determines the vertical velocities (ascending branch of the Brewer-Dobson circulation), whereas convectively-driven transport within the Hadley circulation (red and blue regions near equator) determines the vertical velocities below θ=340 K. In particular, a cooling layer exists in the tropics between 340 and 360 K potential temperature, i.e. on average the air parcels descend rather than ascend in this region. In the polar regions during the winter, increased diabatic descent above 30 hPa indicates the positions of the polar vortices.

The meridional positions of the jets can be deduced from the isolines of the wind (white, solid – westerlies, dashed – easterlies) with a clear signature of STJ (maxima around ζ=360 K) and of the polar jets in the middle stratosphere during the winter. Below the tropopause in the extratropics, the signatures of the Ferrell cells can be seen, which are driven by zonally asymmetric eddies along the poleward flanks of the STJ (e.g. Holton, 1992). It should be noted that because $\zeta\approx p$ below the tropopause, the major part of $\dot{\zeta}$ is associated with adiabatic eddy transport that would vanish if the $\theta-$coordinate were used down to the ground.

Furthermore, the upward velocities in the Ferrell cells reach the extratropical tropopause (the gray contours defining $\dot{\zeta}$=0 cut the blue |PV|=2–4 PVU lines), although this ECMWF-based vertical transport is probably too strong (see $\dot{\zeta}$=0 isoline in the summer hemisphere in September in Fig. 4 extending up to 100 hPa). Thus, in the extratropics, p_r values higher than 100 hPa seem to be more appropriate for the transition level from the radiation- to pressure-related vertical velocities.

2.4 Mixing

As in the previous CLaMS simulations, the initial distribution of air parcels is transported according to trajectories calculated from horizontal ECMWF winds and vertical velocities $\dot{\zeta}$ with subsequent layerwise mixing. This mixing procedure inserts new air parcels into the irregular grid. In particular, such new air parcels are included in those parts of the grid where distances between the next neighbors (calculated before the advection step) have increased above or have fallen below a critical value (for details see Konopka et al., 2003, 2004).

The mixing procedure uses the same optimized mixing parameters as described in Konopka et al. (2004) (critical Lyapunov exponent λ_c=1.5 day^{-1}) and is applied after each advection step Δt=24 h. The critical deformation associated with this advection step is given by $\gamma_c=\lambda_c\Delta t$=1.5. Thus, flow deformations with $\gamma>\gamma_c$ effectively trigger mixing within CLaMS. This spatially and

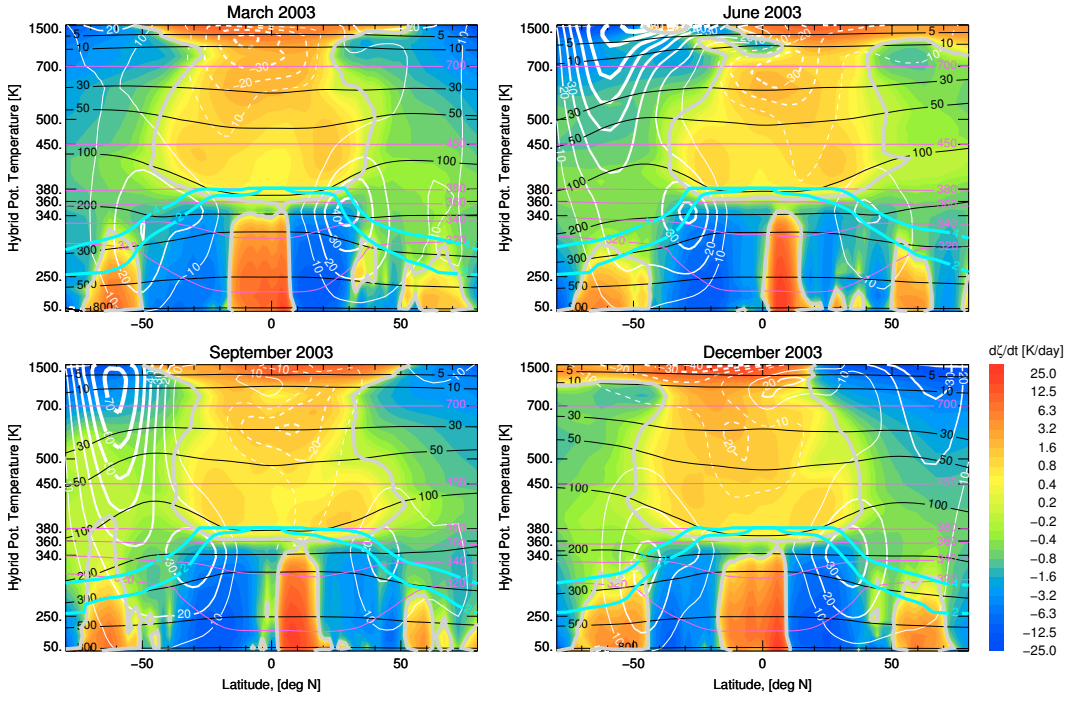

Fig. 4. Zonally and monthly averaged vertical velocities $\dot{\zeta}$ shown as a function of the entropy-weighted hybrid coordinate θ (i.e. the entropy density along the vertical axis is constant). The gray contour defined by $\dot{\zeta} = 0$ separates the ascent from descent regions. White contours (solid – westerlies, dashed – easterlies) describe the zonal wind. The isolines of pressure (black) and potential temperature (pink) are overlaid. The isolines |PV|=2 and 4 PVU together with the θ =380 K line (blue) approximate the position of the tropopause in the extratropics and in the tropics, respectively.

temporally inhomogeneous procedure is driven by strain and shear rates of the horizontal wind with highest values in the vicinity of the jets, in particular in the outer flanks of the polar jet (Konopka et al., 2004, 2005) or in the vicinity of the STJ (Pan et al., 2006).

Let us consider two adjacent air parcels separated by the horizontal and vertical distances r_0 and $\Delta z/2$, respectively, and follow the CLaMS mixing procedure that is applied with the frequency $1/\Delta t$ (here Δt=24 h denotes the length of the pure advection in terms of the trajectories and has nothing to do with the trajectory integration time step that is of the order of 10 min). The (numerical) horizontal and vertical diffusivities of an air parcel involved in a mixing event can be approximated by $D_h \approx r_0^2/4\Delta t$ and $D_v \approx \Delta z^2/4\Delta t$, respectively, and are set to 0 if this air parcel was not affected by mixing. D_h and D_v can be understood as numerical errors of the time and spatial interpolations on the air parcels created by the mixing algorithm, which can also be reinterpreted as the diffusion coefficients of a discretisized diffusion equation (Konopka et al., 2004).

Now, we discuss how CLaMS mixing works within the TTL. In the three panels of Fig. 5, the mean vertical diffusivity D_v per air parcel is shown for ζ=340, 360, 380 K from top to bottom, respectively (blue shaded), as parameterized by the CLaMS mixing algorithm applied for 8 February 2005, after the last advection step. The mean values of D_v are derived from the fraction of air parcels affected by mixing within the grid box with 150 km length. D_v varies between 0 (white) and $\approx$1 m^2/s (dark blue).

Stronger vertical diffusivity D_v (dark blue) can be found in regions with enhanced horizontal velocity (STJs) or, as we will discuss below, in regions with enhanced vertical shear (tropics or STJs). The pattern of the horizontal diffusivity D_h is approximately the same as that of the vertical diffusivity D_v. With $D_h = \alpha^2 D_v$ (Haynes and Anglade, 1997; Konopka et al., 2005), D_h is larger than D_v around the tropical tropopause by approximately a factor $250^2 \approx 10^4$. Because α decreases with distance from the ζ=380 K level, the corresponding values of D_h, relative to D_v, are also smaller.

To show that preferably vertical shear drives CLaMS mixing within the TTL, the integral (Lyapunov exponents) and the local (horizontal and vertical shear) measures of deformations are calculated within the CLaMS layer $\Delta\zeta$ surrounding the ζ=360 K layer (Fig. 6). In particular, the Lyapunov exponents λ were derived from the elongation of a circle with radius r_0 (here 100 km) defined by ten additional air parcels surrounding a given CLaMS air parcel. These additional air parcels are defined either at the surface ζ=360 K or are

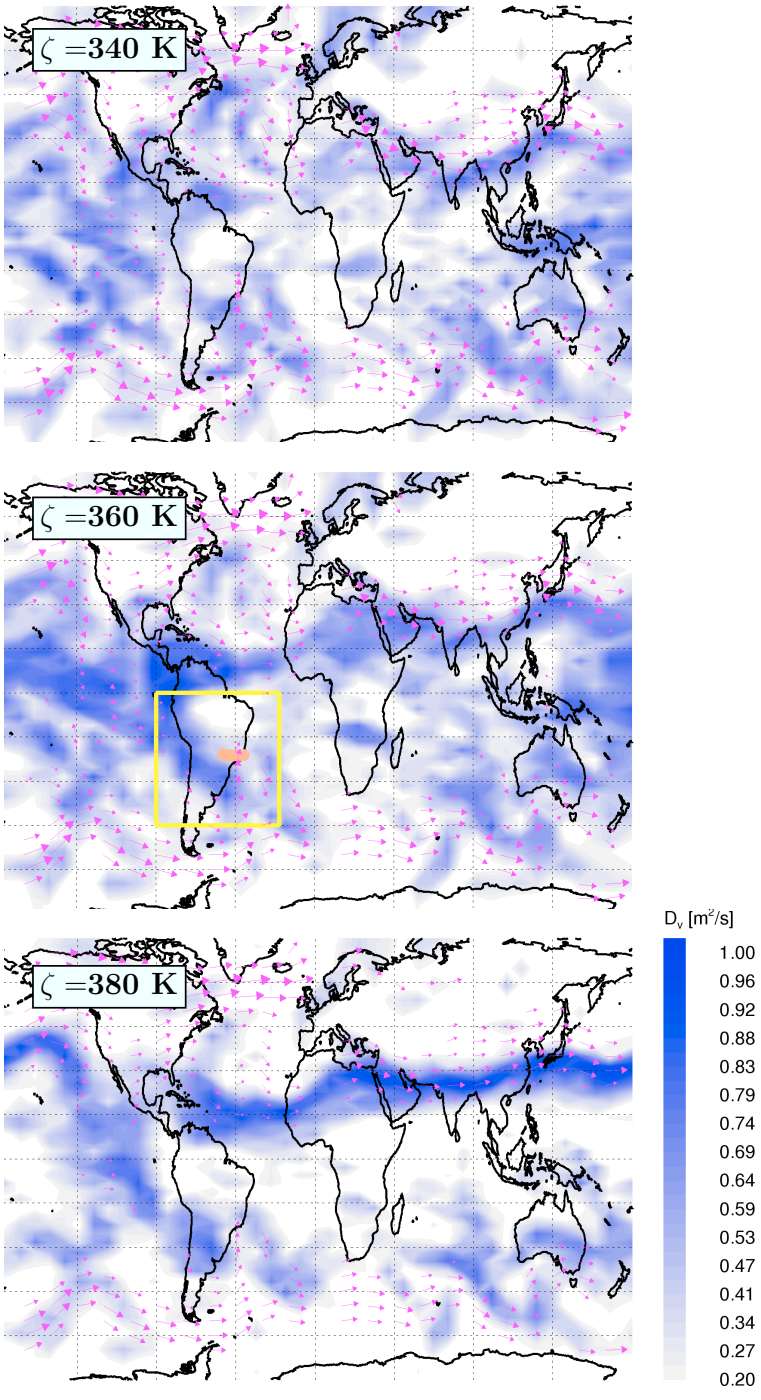

Fig. 5. CLaMS vertical diffusivity D_v on 8.02.2005 at ζ=340, 360 and 380 K from top to bottom as implemented in CLaMS by the deformation-induced mixing procedure (blue shaded). Wind vectors (pink) are plotted for wind velocities higher than 20 m/s. The TROCCINOX flights took place in the region framed in yellow, in particular the Geophysica flight on 8 February 2005 (beige) that will be discussed below.

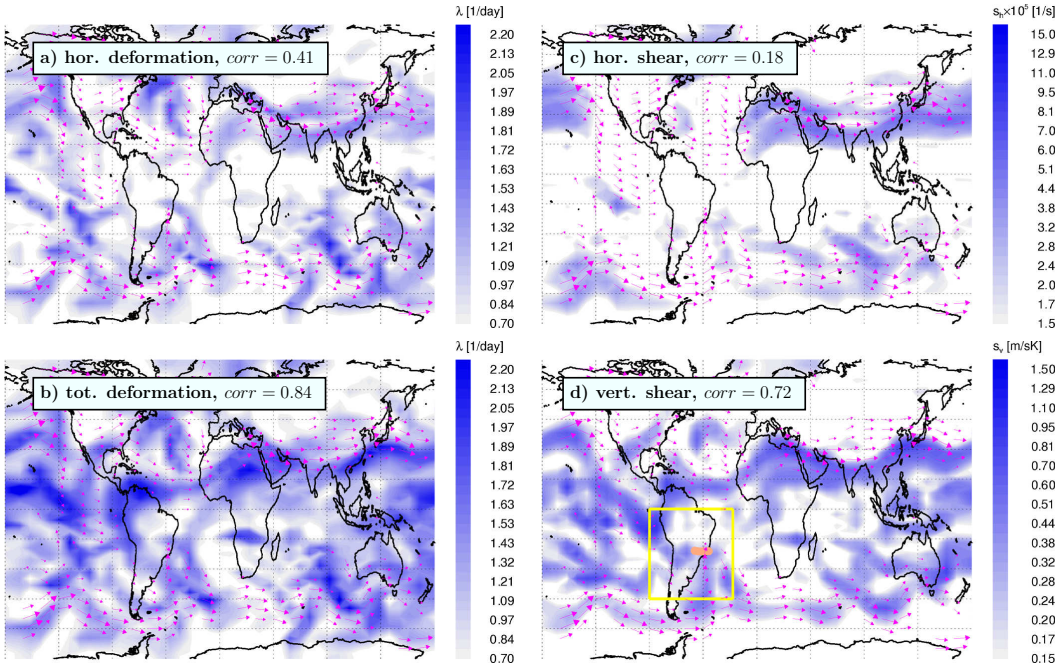

Fig. 6. Measures of deformation at ζ=360 K calculated in terms of the horizontal **(a)**, total **(b)** deformations quantified by the Lyapunov exponents and in terms of the horizontal **(c)** and vertical **(d)** shear. Correlation coefficients are calculated between the mean vertical diffusivity D_v (middle panel of Fig. 5) and the respective measures of deformation. In the region framed in yellow, the TROCCINOX flights took place, in particular the Geophysica flight on 8 February 2005 (beige). As we discuss below, the air composition during the flight segment around θ=360 K was influenced by aged convection caused by MCS over Argentina and South Brazil.

uniformly distributed within the layer $\Delta\zeta$=15 K around the ζ=360 K surface.

While in the first case only horizontal deformations lead to increased values of λ, in the 3-D case the combined effect of horizontal strain and vertical shear causes significantly higher total deformations and, consequently, higher values of λ. The corresponding mean Lyapunov exponents λ shown in Figs. 6a and b were derived from 24-h forward trajectories started on 7 February 2005 and averaged over the same grid on which D_v was determined in Fig. 5.

In contrast to these integral (Lagrangian) measures of deformation, the local (Eulerian) horizontal and vertical shear rates are shown in the right column of Fig. 6. The horizontal shear (in 1/s) was determined from the absolute change of the wind perpendicular to the wind direction (Fig. 6c) whereas the vertical shear (in m/sK) plotted in Fig. 6d was derived from the difference of the horizontal wind in the layer above and below the considered layer. Both quantities were averaged over five ECMWF data sets within the considered 24-h time interval and over the same grid as the Lyapunov exponents.

Correlation coefficients calculated between the mean vertical diffusivity D_v (middle panel of Fig. 5) and the four parameters discussed (Fig. 6a to d) amount to 0.4, 0.8, 0.2, and 0.7 for the horizontal and total deformations as well as for the horizontal and vertical shear, respectively. The values of the coefficients calculated in the same way for ζ=340/360 K are given as 0.6/0.5, 0.8/0.8, 0.2/0.3 and 0.6/0.8, respectively.

As expected, the highest correlation coefficient was achieved for the case considering the total deformations measured in terms of the 3-D Lyapunov exponent, because the total integral deformation is the underlying driving force that triggers the mixing algorithm in CLaMS (Konopka et al., 2004, 2005). However, a remarkably high correlation could be achieved between the CLaMS mixing intensity and the vertical shear (Fig. 6d). Whereas in the vicinity of the STJs, mainly vertical but also horizontal shear correlates fairly well with the corresponding distribution of D_v (middle panel of Fig. 5), regions with enhanced mixing within the tropics are dominated by the vertical shear, to some extent in the outflow regions of strong convection (see Fig. 3), in particular over Indonesia, the south-eastern Pacific, Central Africa, Madagascar and also Brazil (yellow framed region in Fig. 6d).

In the case of convection over Brazil, strong thunderstorms were reported over Argentina and South Brazil during the three days before the Geophysica penetrated the outflow of these aged MCS. As discussed below (Sect. 5.2), the associated MCSs, here in connection with the STJ that was displaced southward by the Bolivian high, influenced the upper tropospheric flow on the tropical side of the jet. This kind

of coupling between the deep convection and the upper tropospheric flow was recently discussed in connection with the Asian summer monsoon anticyclone (Randel and Park, 2006) that has some similarities with flow generated around the Bolivian high (Zhou and Lau, 1998). Thus, CLaMS transport in the TTL shows strong mixing in the vicinity of the STJs and, to some extent, in the outflow regions of the large-scale convection, i.e., these locations are favored for mixing-induced vertical transport.

2.5 Boundary conditions

In addition to the initial conditions that will be described in the next section, boundary conditions need to be specified for the CLaMS model domain. After each mixing procedure, the air parcels in the top level of the model are replaced by their initial geometric configuration. Furthermore, the mixing ratios are set to prescribed values as given by the HALOE climatology, Mainz-2-D model or by some additional conditions (e.g. tracer-tracer correlations, (Grooß et al., 2005)). Also the air parcels with $\zeta_0<\zeta<\zeta_0+\Delta\zeta_0$ with $\Delta\zeta_0$=50 K and ζ_0 defined by the surface that follows the orography at the bottom of the model domain are replaced be their initial geometric positions. Their mixing ratios are either redefined in a manner similar to the upper boundary or are interpolated from their next neighbors and can be updated according to prescribed fluxes.

The use of the pressure-like coordinate below the tropopause, $\eta=p/p_0$ instead of $\sigma=p/p_{\mathrm{surf}}$, i.e. a terrain-following coordinate (see Eq. 1), is motivated solely by the simplicity of this coordinate in a Lagrangian CTM. In Eulerian models, the use of the σ coordinate allows to define a compact surface as the lower boundary of the model at which boundary conditions can be formulated. In contrast, the Lagrangian approach and in particular the use of the CLaMS hybrid $\zeta-$ coordinate, allows to define the boundary conditions within a layer $\Delta\zeta$ following the orography even if some model layers intersect this terrain-following layer. If the ECMWF velocities are correct, the trajectories of the air parcels should overcome all possible orographic obstacles. However, if any air parcel leaves the model domain the mixing algorithm creates a new one by filling the resulting hole. The mixing ratio of this air parcel is interpolated from the next available neighbors.

Thus, in contrast to the Eulerian approach, it is not necessary to have a single, terrain-following surface as the lowest boundary of the model. Nevertheless, some studies comparing the positions of trajectories calculated in σ-coordinates (FLEXPART) with the corresponding positions in p-coordinates (LAGRANTO) show some advantages, mainly due to an improved interpolation technique (Stohl et al., 2001). In summary, while our treatment of the lower boundary might possibly cause some problems calculating mixing ratios in the boundary layer, it will have no impact on the CLaMS simulations within the TTL.

3 Validation of CLaMS transport by TROCCINOX measurements

To validate the properties of transport associated with the new hybrid coordinate ζ, we use in situ data measured during the TROCCINOX campaign on board the high altitude Russian aircraft, Geophysica. The campaign took place in early 2005 in Araçatuba (21.2° S, 50.4° W), Brazil, with 8 local and 8 transfer flights extending up to an altitude of 20 km (or up to $\theta\approx$450 K), i.e. covering the TTL region very well.

The experimental data used in this paper were sampled with FOZAN (ozone), FISH (total and gas phase water), HAGAR (CH_4), SIOUX (NO, NO_y) and COLD (CO) instruments. A detailed description of the instruments can be found in Stefanutti et al. (2004) and Voigt et al. (2005) for the SIOUX instrument.

3.1 Meteorological situation

The composition of tropical air in the vicinity of the tropopause over Araçatuba was frequently influenced by the interaction between the upper-level, quasi-stationary Bolivian high (BH) with STJ (see Fig. 7) surrounding the Bolivian high southerly. Zhou and Lau (1998) reported the existence of high-level southerlies over South America during the austral summer, which were influenced by the Bolivian high, and pointed out some similarities of this circulation pattern with the well-known summer monsoon circulation over south-east Asia (e.g., Dethof et al., 1999; Randel and Park, 2006).

The air over Araçatuba was influenced by numerous MCSs that frequently formed over the southeast of South America (north Argentina, south Brazil, part of Paraguay and part of Uruguay). These air masses were transported along the STJ, often displaced by the high-level southerlies, to a region within the Geophysica range. In addition, isolated thunderstorms in the vicinity of Araçatuba were also observed by the Brazilian radar network.

The eight local flights during the campaign can be divided into 3 groups: 4 flights in almost pure tropical air, northwards of the STJ on 12, 15, 17 and 18 February, 2 flights above and within isolated thunderstorms on 4 and 5 February, and 2 flights on 1 and 8 February in air masses strongly affected by the aged MCS and STJ. Because in contrast to the MCS, the isolated convective systems such as those on 4 and 5 February are not resolved by the ECMWF large-scale analysis, we focus our analysis on the flights on 1 and 8 February as examples of the STT and TST processes, respectively (Fig. 7 top and bottom). But first we describe the setup of CLaMS used for this study.

3.2 Configuration of CLaMS

The high-resolution (50 km horizontally and up to 200 m vertically around the tropical tropopause) version of CLaMS as

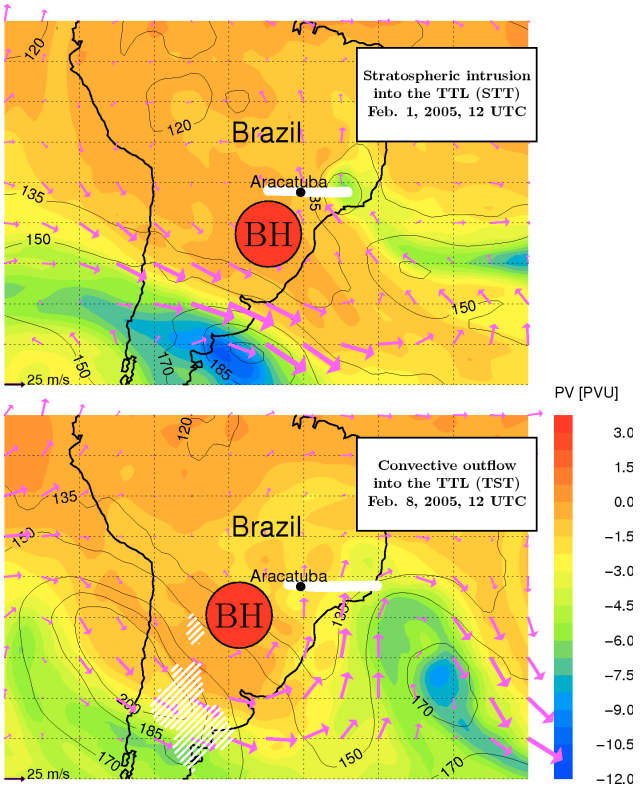

Fig. 7. Map of ECMWF potential vorticity (PV) at θ=360 K on 1 February (top) and on 8 February, 12:00 UT (bottom). On these 2 days, signatures of stratosphere-troposphere exchange were observed (thick white lines denote the flight tracks). Pink arrows show the horizontal wind with highest values across the subtropical jet (STJ) surrounding the upper-level, quasi-stationary Bolivian high (BH). The black lines are pressure isolines (in hPa). Top: Air masses with low PV values (blue) east of Araçatuba are trapped in the TTL by a cut-off low. These air masses had been separated from the lowermost stratosphere, transported along the STJ and mixed into the TTL (stratosphere-to-troposphere transport, STT). Bottom: MCS over Argentina and South Brazil (white dashed contours denote regions with ECMWF-H_2O >25 ppmv on 7 February, 06:00 UT, i.e. about 32 h prior to the flight) transports air masses from the boundary layer up to about 330–340 K. Vertical mixing along the STJ lifts these air masses up to about 360 K, where cirrus clouds, enhanced water vapor, and increased NO/NO_y ratios were observed (troposphere-to-stratosphere transport, TST).

described in the previous section is used to transport O_3 and N_2O as passive tracers without any chemical change. The model was initialized globally, between the earth's surface and ζ=1400 K, for 20 November 2004, using MLS observations (O_3, N_2O) and the Mainz-2-D model above and below ζ=400 K, respectively (Grooß and Müller, 2007).

Two artificial tracers are used to mark air masses with different origins. In particular, the stratospheric tracer (ST) is set to 100% at the initialization time in the domain defined by ζ>380 in the tropics (i.e. within the latitude range between 20° S and 20° N) and by |PV|>2 PVU elsewhere. At the top CLaMS level, ST is kept constant during the entire simulation. The ST value of a given air parcel can change only due to mixing and, consequently, this value quantifies the percentage of stratospheric air within this air mass. Similarly, the boundary layer tracer (BT) is re-initialized every 24 h to 100% within the lowest layer with the thickness $\Delta\zeta$=50 K that follows the orography. Thus, high BT values in the upper troposphere indicate a fast vertical transport driven by convection.

To understand the impact of mixing on the transport of trace species we run CLaMS in two configurations: without mixing (i.e. transport only in terms of forward trajectories) and with mixing by using mixing parameters described in Sect. 2.4.

4 Stratospheric intrusion into the tropical tropopause layer (TTL)

During the flight on 1 February, tracer signatures of a deep stratospheric intrusion into the TTL were observed. This intrusion (cut-off low) was formed as a tongue of low PV (see Fig. 7, top panel) that had been separated from the stratosphere and quasi-isentropically transported into the TTL on a time scale of several days by a meandering and relatively weak STJ.

Occasionally, the meandering STJ that surrounds the Bolivian high becomes unstable (usually when the Bolivian high is displaced eastwards) due to a breaking Rossby wave and, consequently, bifurcates into two branches. Whereas the main branch follows the main eastward direction, a secondary branch flows anticlockwise around the Bolivian high and mixes into the TTL.

Along the flight track (Fig. 8, top panel), spikes of enhanced ozone (black arrows) were observed several times by the FOZAN instrument (black) clearly below the tropopause (defined here as |PV|=2 PVU surface). These signatures were successfully reproduced with CLaMS (colored line), with better agreement than the assimilated ozone provided by ECMWF (pink). The colors of the CLaMS line denote the percentage of ST. CLaMS results with mixing switched off (gray) strongly overestimate the observed ozone values, in particular below the tropopause indicating too weak upward (or too strong downward) transport in pure trajectory studies. Alternatively, in reality, the stratospheric (high ozone) signatures might be destroyed by mixing with tropospheric air, a process that is neglected in a pure trajectory study.

The vertical ST distribution above and below the flight track together with |PV|=2 PVU (tropopause) and Q=0 (clear sky radiative equilibrium) are shown in the bottom left panel of Fig. 8. The spatial distribution of ST extends down to about 500 hPa. The position of the meandering STJ (see also Fig. 7) can be inferred from the isotachs of the horizontal wind (light gray). A strong STT signal observed during this

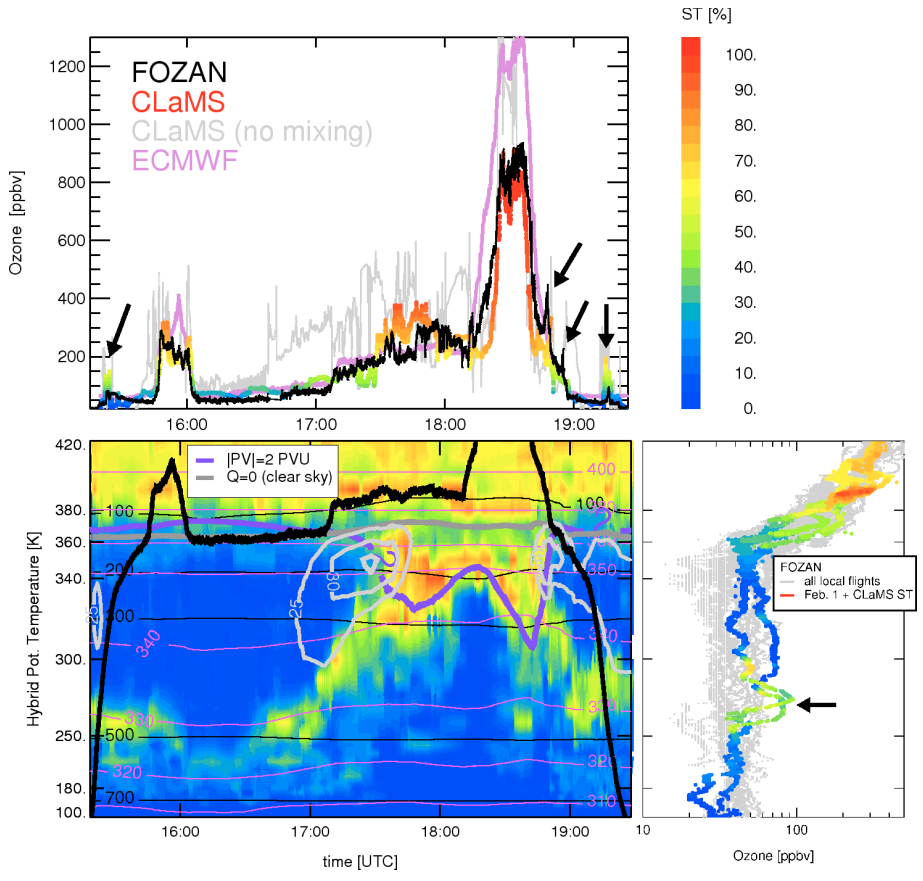

Fig. 8. Top: Ozone observations (FOZAN black, ECMWF pink) and CLaMS simulations colored with the percentage of the stratospheric tracer ST within the observed air masses as modeled by CLaMS during the flight on 1 February. Bottom left: The vertical distribution of ST along the flight track. Thin black and pink lines are p and θ-isolines, respectively. The tropopause defined as |PV|=2 PVU surface (violet), the $Q = 0$ level (dark gray) and the isotachs (light gray) indicating the position of the STJ are also shown. Bottom right: FOZAN profiles as observed during all local flights (gray) compared with the profile measured on 1 February and colored with ST.

flight can also be seen by a comparison of the ozone profiles with all other profiles measured during the campaign (bottom right panel of Fig. 8). The profiles measured on 1 February, which are also colored with ST, show strong stratospheric signatures around ζ=250 K (≈500 hPa) with ozone values around 100 ppbv (black arrow). This is a significantly higher value than all other tropospheric ozone values measured during the campaign (gray lines).

To some extent, the STJ still isolates stratospheric intrusion from the tropical air while the remnants of this intrusion are mixed into the troposphere, mainly below the jet. Relatively good agreement between the observed and simulated filaments (black arrows in the top panel of Fig. 8) and the position of the stratospheric remnants shows the ability of CLaMS to reproduce small-scale structures within the TTL.

Overall good agreement between the simulated and observed O_3 and CH_4 time series was achieved for all local flights with correlation coefficients of 0.89 and 0.86, respectively. The passively transported O_3 slightly underestimates the observed values in the lower stratosphere indicating that, as expected in the tropics, chemical ozone production might improve the agreement in full chemistry studies. Near the tropopause, ozone assimilated by ECMWF shows astonishingly good agreement with the FOZAN data. In the stratosphere, ECMWF-O_3 overestimates the observation, with a linearly increasing error from 5% around θ=380 K up to 40% at θ=450 K.

5 Troposphere-to-stratosphere transport along the subtropical jet

The flight on 8 February permits a study of the reverse process to that discussed above, namely the transport of tropospheric air into the stratosphere (TST). During the outbound flight leg between 13:45 and 15:30 UT, the TTL was penetrated at around θ≈360 K (see Fig. 7, bottom panel). The flight leg under consideration starts slightly below the |PV|=2 PVU surface over Araçatuba and leads toward the

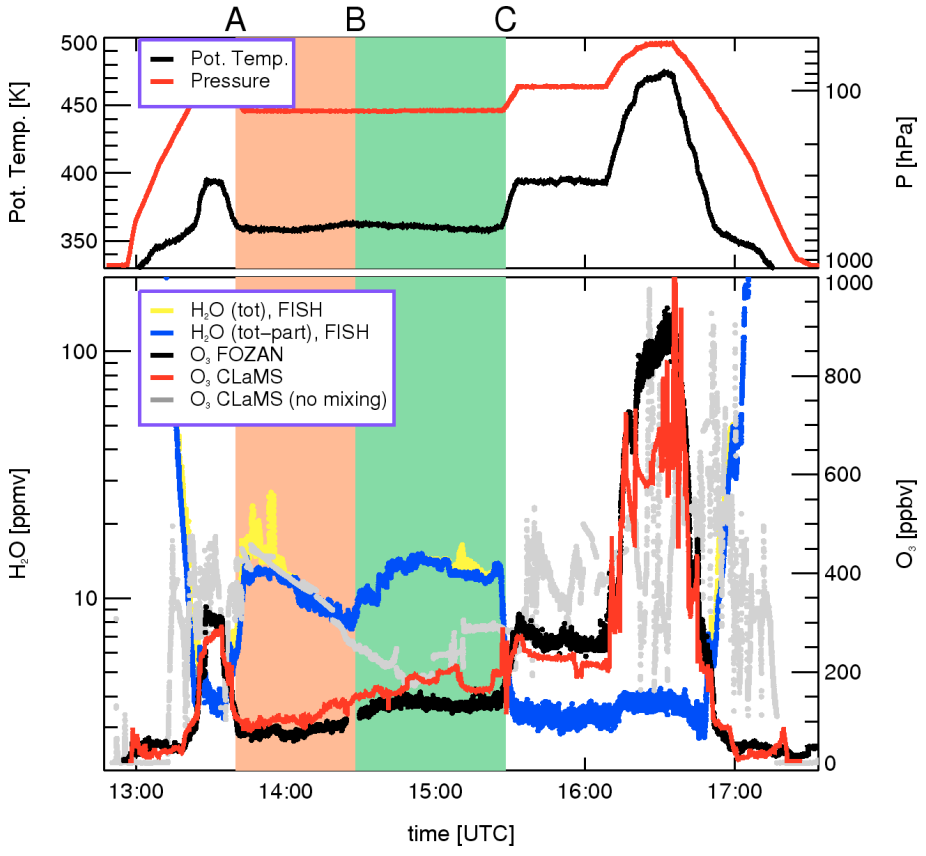

Fig. 9. Flight on 8 February. Top: Potential temperature (black) and pressure (red) along the flight track. Bottom: Total water (yellow) and water vapor (blue) as observed by the FISH instrument. Furthermore, observed (black) and simulated ozone with (red) and without mixing (gray). In the beige (AB) and green (BC) segments of the flight ($\theta \approx 360$ K), signatures of stratosphere-troposphere exchange were observed with an increasing stratospheric contribution. According to CLaMS, these contribution can be explained as a consequence of mixing within the TTL disturbed by the STJ.

STJ core around the easternmost point of the flight track with |PV|>3 PVU and wind velocities higher than 35 m/s (see also Fig. 13).

Along this leg (see Fig. 9), signatures of mixing were detected with at first more tropospheric and then more stratospheric contribution observed in the beige (AB) and in the green (BC) colored time intervals, respectively. In particular, enhanced values of total water (up to 30 ppmv, yellow) and water vapor (up to 15 ppmv, blue) were detected by the FISH instrument at a pressure level of 125 hPa, i.e. slightly above θ=360 K. A positive difference between the total water and water vapor (derived from the temperature and 100% ice saturation assumption) indicates the existence of cirrus clouds. This signature can be seen twice, shortly before 14:00 and a small spike after 15:00 UTC.

Surprisingly, after about 14:30 UT (BC), enhanced ozone values (up to 150 ppbv, FOZAN) were detected (black), indicating increasing stratospheric influence. This transition from the tropospheric (AB) to more stratospheric O_3 mixing ratios (BC) is also reproduced by CLaMS simulations with mixing (red). On the other hand, pure trajectory calculations (gray) significantly overestimate the observed ozone values showing that such calculations do not correctly represent the upward transport.

The simultaneous presence of the tropospheric and stratospheric signatures in the air masses sampled on February 8 (and February 1) can also be seen in Fig. 10 where the profiles of the total water (a) as well as the correlations of ozone with total water (b) and with NO/NO_y (c) are compared with other pure tropical flights (black versus gray). Thus, significantly higher values of H_2O were observed within the TTL affected by the STJ (black) than within the tropical TTL far away from the STJ (gray). In particular, as can be deduced from the ozone/total water correlation, the air masses sampled along the entire ABC leg were influenced by mixing between the troposphere and stratosphere (relatively strong deviation of the observed correlations from an ideal, unmixed, L-shaped correlation) with much higher stratospheric influence along the BC than along the AB part of the leg.

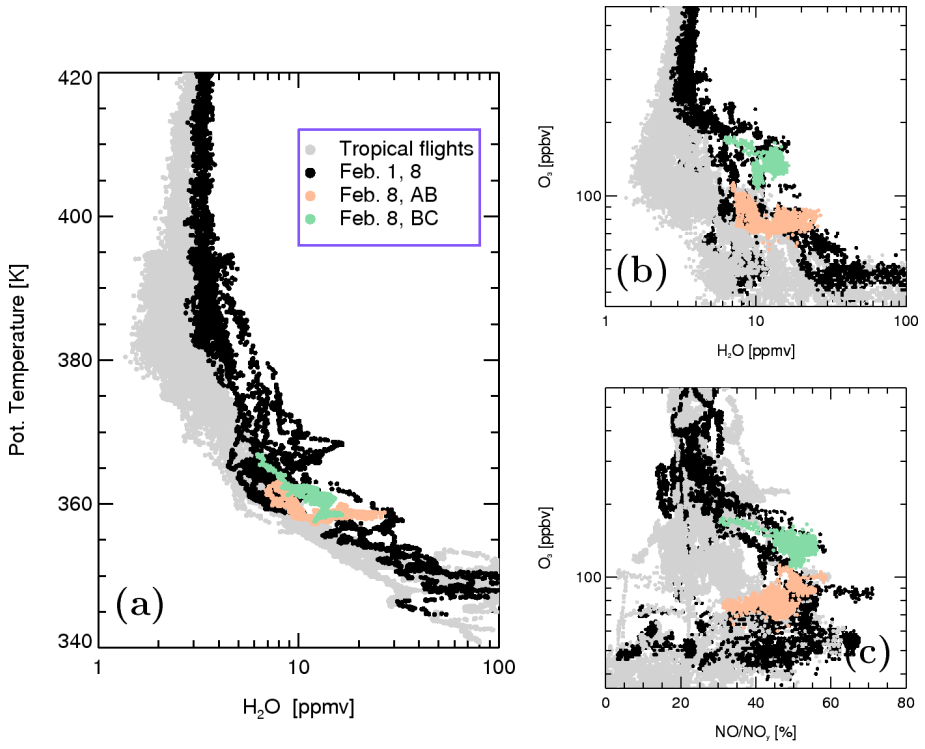

Fig. 10. Profiles of total water **(a)**, correlations of ozone with total water **(b)** and with NO/NO_y **(c)** during the flight on 8 February and 1 February (black) compared with pure tropical flights far away from fresh convective systems (gray). The contributions from the AB and BC flight segments are colored beige and green, respectively.

Furthermore, comparatively high ratios of NO/NO_y (30–55%) were observed along the entire ABC segment that indicates contributions of relatively fresh lightning. Based on observations around 200 hPa, Schumann et al. (2004) report that ratios between 30 and 50% are signatures of lightning no older than 3 h. Because the lifetime of NO_x at 125 hPa is longer by about a factor 10 than at 200 hPa (Tie et al., 2001, 2002), the observed NO/NO_y ratios may be typical of an elapsed time of the order of few days. Using trajectory analysis, we now discuss the origin of these air masses.

5.1 Trajectory analysis

A common way to trace back the origin of the sampled air masses is to use backward trajectories starting from the flight track (see Fig. 11, top panel). Here, the positions and the ECMWF H_2O mixing ratios along 3-day backward trajectories are shown. The trajectories were calculated using ζ-coordinates and the CLaMS trajectory module driven by the 6-h ECMWF analysis data.

The trajectories show high ECMWF H_2O values of about 50 ppmv about 30 h before the flight whereas about 40 h prior the flight H_2O values of less than 7 ppmv were found in these air masses. Furthermore, the potential temperature did not significantly change along these trajectories (the absolute variation is less than 2 K) indicating an almost isentropic transport. Because the trajectories do not descend below ≈200 hPa, the diagnosed high ECMWF H_2O values are probably caused by the sub-grid parameterization of convection in the ECMWF model.

Similar results were also found with the FLEXPART model (Ren et al., 2007) and with LAGRANTO trajectories driven by 3-h ECMWF data (Wernli and Davies, 1997), even if some of those backward trajectories reached the 220 hPa level. Furthermore, for all flight legs on 1, 4, 5 and 8 February with $350<\theta<380$, the corresponding backward trajectories, calculated both with CLaMS and LAGRANTO, do not descend below ≈300 hPa for the previous 5 days, even on 4 and 5 February when the observed air masses were strongly influenced by fresh convection. The small discrepancies between CLaMS and LAGRANTO likely originate from the differences in the applied ECMWF data (6- versus 3-h frequency) rather than from the differences in the trajectory advection schemes.

The vertical displacement of the backward trajectories changes significantly if their start positions are shifted down below the flight track by 25 K. In the bottom panel of Fig. 11, the horizontal coordinates of the 3-day backward trajectories are shown, which were initialized 25 K below the flight leg ABC on 8 February (i.e. 25 K below the beige and green time

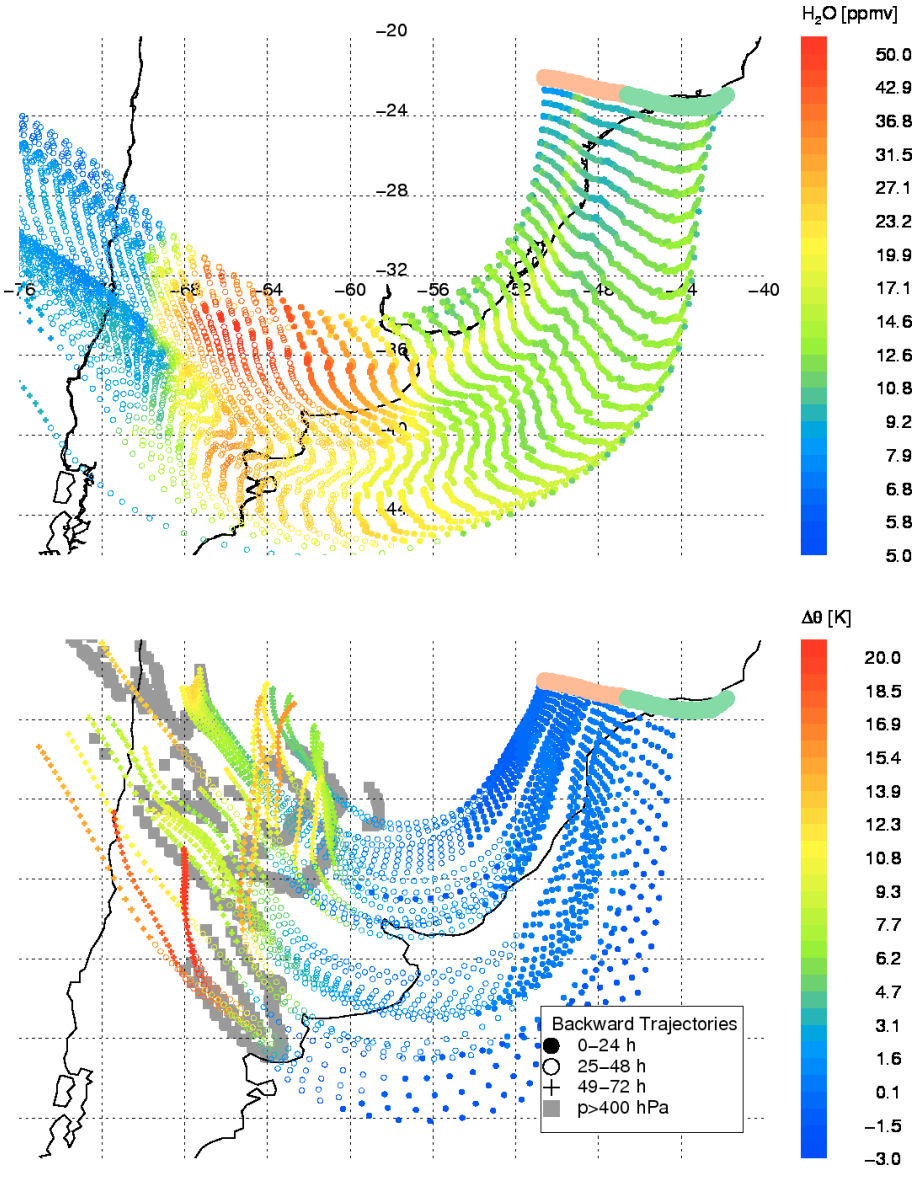

Fig. 11. 3-day backward trajectories starting on 8 February 2005 between 13:45 and 15:30 UT from the AB (beige) and BC (green) flight legs (top) or 25 K below these flight legs (bottom). Top: ECMWF H_2O interpolated along these trajectories. Bottom: $\Delta\theta$ experienced by the air masses along the backward trajectories starting 25 K below the flight track. Positive (red) and negative (blue) values correspond to up- and downward motion of air with increasing time. The gray footprints are places where the trajectories cross the 400 hPa level. In the satellite pictures (GOES), fresh convective clouds could be found in the same region (see Fig. 12).

segments). The positive (negative) values of $\Delta\theta$ along the trajectories denote their total ascent (descent) with increasing time. The gray footprints show the positions where these trajectories cross the 400 hPa level and, in the following, these positions are interpreted as regions where convection lifted the corresponding air masses. The age of convection can be derived from the trajectory length (see legend in Fig. 11) and varies between 30 and 70 h for the southern- and western-most footprints, respectively.

Such an interpretation of the footprints is supported by the infrared (chanel 4) GOES-East satellite pictures (Fig. 12), which show a convective cloud covering 53, 40, and 30 h before the flight at approximately the same locations as inferred from the trajectory calculations. Thus, it seems that two MCS, the older one over the northeast of south of Brazil and part of Uruguay (beige) and the younger one over Argentina (green), contributed to the tropospheric signatures in the respective AB and BC parts of the considered flight leg. A different origin of these air masses is also manifested in

a discontinuity in the measured time series of water vapor around 14:30 UT (see Fig. 9). This discontinuity can also be seen in the time series of temperature (first part of the leg is colder by ≈3 K) and the relative humidity (not shown).

5.2 Contribution of mixing

Thus, the question arises of the reason that trajectory analysis can explain the convection-induced tropospheric signatures at most up to $\theta \approx 340$ K but not the observed relatively fresh tropospheric signatures (enhanced NO/NO_y ratio and cirrus clouds) found slightly above 360 K. As a first hypothesis, it is possible that $\dot{\zeta}$ derived from the large-scale ECMWF vertical velocity are underestimated in regions affected by convection.

To some extent, this hypothesis is supported by observations of CO by the COLD instrument on 4 February with a maximum mixing ratio of ≈140 ppbv extending up to about 360 K in air masses within and slightly above an isolated convective cell (unfortunately, there are no observations of CO on 1 and 8 February and the quality of the CLaMS CO distribution is strongly limited by a very uncertain data base of CO sources, in particular in South America). Within CLaMS, the highest impact of convection can be defined as the highest level reached by undiluted values of BT (i.e. ≈100%). For all flights when CO is available, this level was found by about $\theta = 350$ K, i.e. about 10 K below the highest convective outflow derived from CO observations.

However, the underestimation of the convective outflow by $\Delta\theta \approx 10$ K does not completely explain the discrepancy between the backward trajectory analysis that started 25 K below the flight level and the observed, relatively fresh tropospheric signatures at $\theta \approx 360$ K. In the remaining part of this section, we show that mixing, in particular that implemented in CLaMS, has the potential to close this gap.

To explore this hypothesis, an additional CLaMS simulation was performed, with BT re-initialized 3 days before the flight to 100% and 0 above and below 400 hPa, respectively. In this way, we redefine BT as a tropospheric tracer and ask if during the following 3 days convection and mixing can lift this tracer up to about $\theta = 360$ K. The results are plotted as a curtain along the flight track in Fig. 13.

Here, BT extends well above $\theta = 335$ K, i.e. well above the maximum of the upward transport as inferred from the pure trajectory analysis shown in Fig. 11. In particular, the BL signature extends up to the AB part of the leg around 14:00 UT (beige), but never reaches the BC part of the leg (green) getting no closer than 10 K below the flight level at 14:45 UT. The position of the first BT signature (beige arrow) roughly coincides with the position of the cirrus clouds (yellow in the beige part of the flight track in Fig. 9).

In addition, the distribution of the stratospheric tracer (not shown) that can be approximated by ST≈100%-BT coincides with the increasing stratospheric properties of the sampled air masses as the Geophysica comes closer to the STJ (illustrated here by the isotachs of the horizontal wind, light gray). The aircraft crosses the $|PV| = 2$ PVU tropopause around 14:00 UT (the violet line denotes the tropopause in Fig. 13), with an increasing stratospheric character of the sampled air along the BC part of the flight leg. Thus,

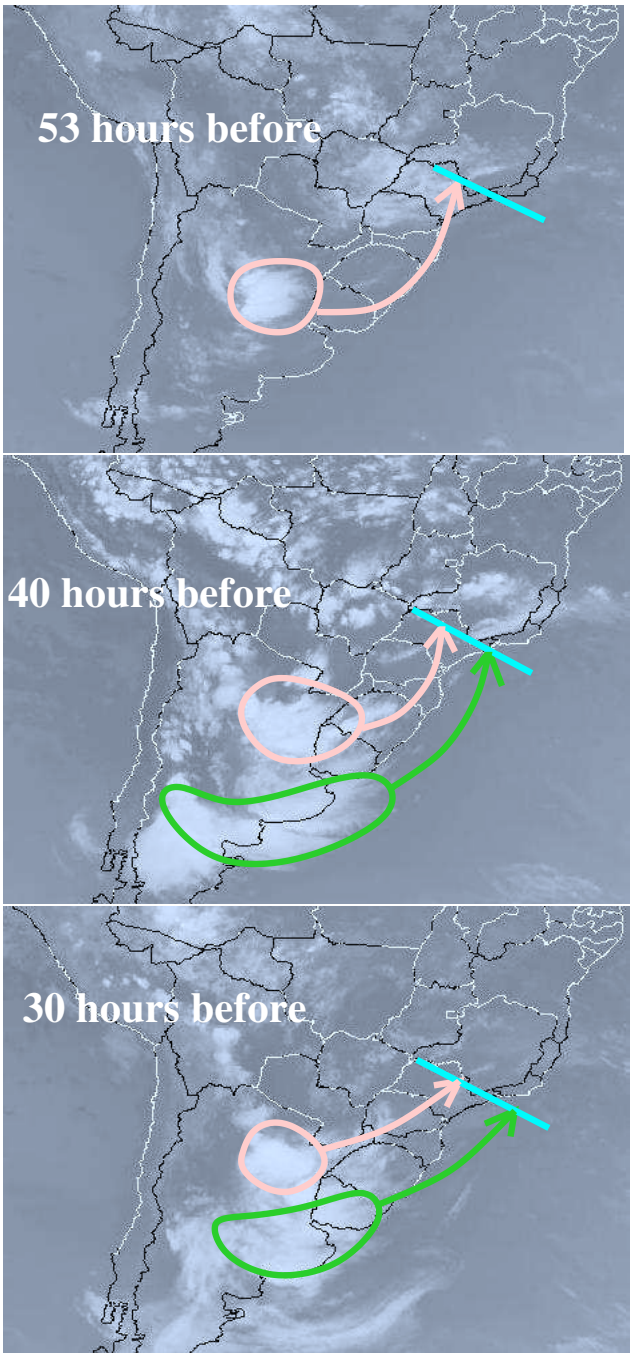

Fig. 12. High clouds indicating convection as detected by the GEOS satellite 53 (top), 40 (middle) and 30 h (bottom) prior to the flight on 8 February.

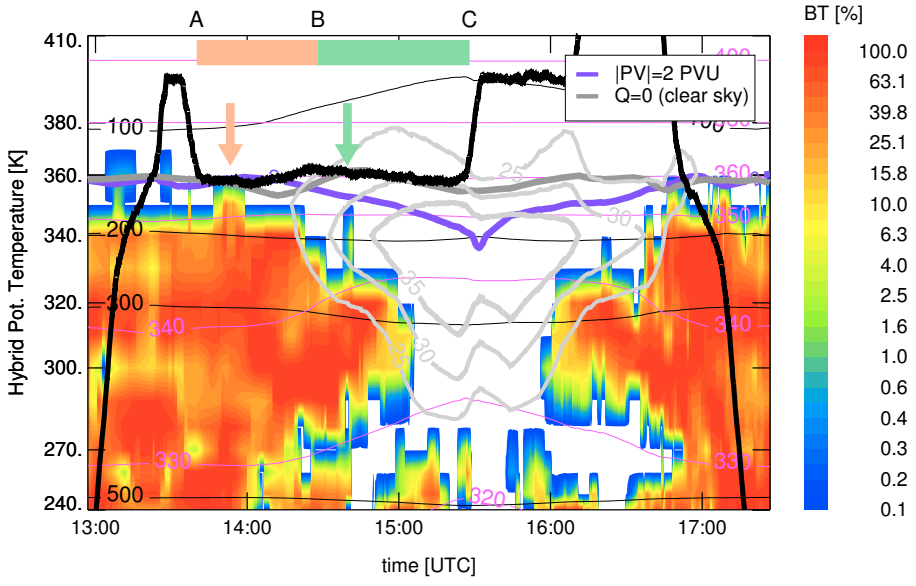

Fig. 13. Vertical distribution of the boundary layer tracer (BT) along the flight track on 8 February 2005. Here, BT was re-initialized 3 days before the flight to 100% and 0 above and below 400 hPa, respectively. The distribution of this tracer shows that mixing has the potential to lift the air masses from the convective outflow around θ=335 K up to 360 K (white means no BT contribution in this region). The tropopause (|PV|=2 PVU, violet), the Q=0 level (dark gray) and the isotachs (light gray) indicating the position of the STJ are also shown.

in agreement with observed and simulated O_3 time series (Fig. 9), the stratospheric contribution increases during the considered flight leg as the Geophysica approaches the jet core. At the end of the second part of the leg (point C), slightly above the tropopause, BT and ST tracers transported over the entire period of 3 months show the weakest tropospheric impact and the strongest contribution of air originating in the lowermost stratosphere, respectively.

We conclude that vertical and isentropic mixing as implemented in CLaMS goes beyond the pure trajectory calculations and explain, at least qualitatively, the observed signatures in the TROCCINOX observations. In the following section, we will discus some additional arguments supporting this hypothesis.

6 Mixing-driven transport in the TTL

To support the argument that mixing in CLaMS does play a crucial role in lifting tropospheric air from the convective outflow around 350 K up to the tropical tropopause around 380 K, we now discuss in Fig. 14 the horizontal (top row) and zonally averaged vertical (bottom row) distributions of BT after more than 3 months of transport (108 days) with and without mixing.

In the case without mixing, pure advective transport along the trajectories occurs. The trajectories are calculated in ζ−coordinates, i.e. by the use of hybrid vertical velocities $\dot{\zeta}$. The horizontal distributions in the top row of Fig. 14 show air parcels within the layer around ζ=380 K. The beige lines are the isotachs of the total and zonal wind in the horizontal and vertical cross sections, respectively, and illustrate the positions of STJ on the last day of the simulation period (i.e. on 7 March 2005). The blue lines in the bottom row indicate the position of the tropopause and are inferred from the |PV|=2–4 isolines in the extratropics and θ=380 K in the tropics.

The large white gaps where air parcels are absent in the left top panel of Fig. 14 illustrate that insufficient number of air parcels ascending in the tropics, or, in other words, that the upward transport driven by convection (from ECMWF) and by radiation (clear sky) is too weak to transport tropospheric species up to the tropical tropopause at $\theta \approx \zeta$=380 K (we later discuss that these white gaps are due to an invalid continuity equation in the ζ−coordinate system). By contrast, the full CLaMS simulations with mixing (top right panel of Fig. 14) show a clear, filamentary signature of upward transport within the tropics laterally confined between the northern and southern STJ and with highest BT values in the tropics over Indonesia and south of the equator over the western Pacific.

The zonally averaged vertical distribution of the BT tracer shown in the bottom right panel of Fig. 14 also illustrates a clear signature of mixing if compared with the results of a pure trajectory transport (bottom left). The vertical mixing strongly affects the TTL region above $\zeta \approx$360 K. Furthermore, a stronger convective activity and a weaker STJ in the summer hemisphere effectively fill the Southern Hemisphere lowermost stratosphere with tropospheric air whereas in the

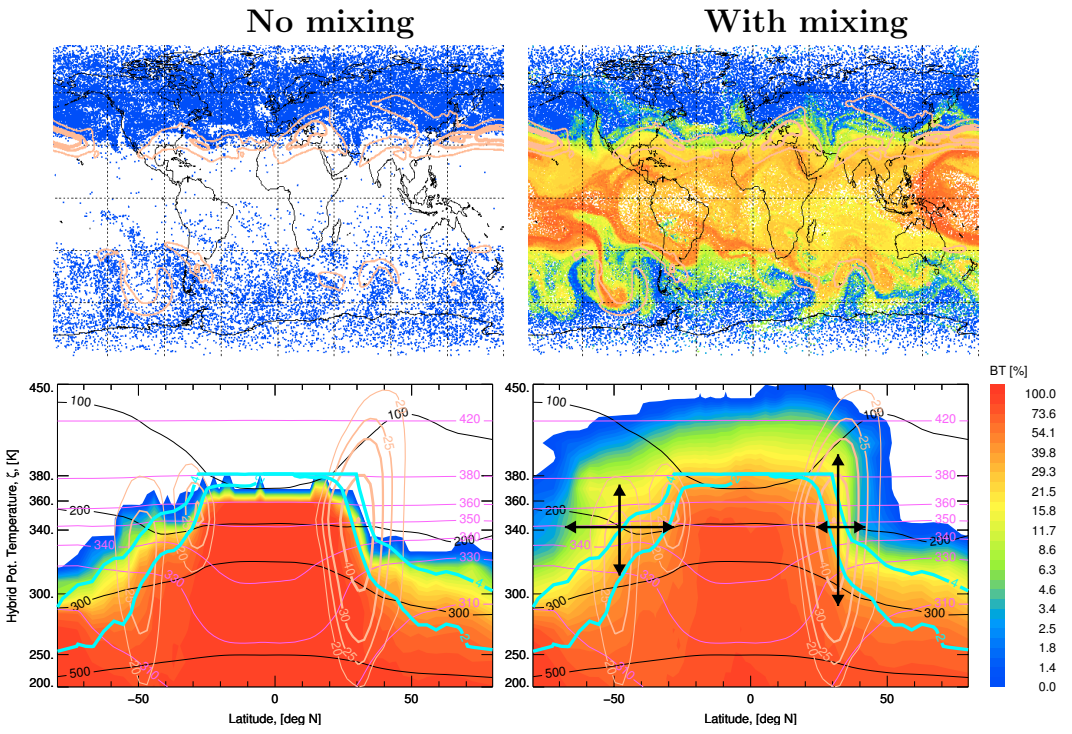

Fig. 14. Horizontal distribution of CLaMS boundary layer tracer (BT) at ζ=380 K (top row) and its zonally averaged vertical distribution (bottom row) after more than 3 months of transport (108 days) on 7 March 2005 calculated without (left) and with (right) mixing.

Northern Hemisphere a stronger STJ combined with an enhanced diabatic descent into the lowermost stratosphere hinder an effective TST.

The meridional distribution of the fraction of CLaMS air parcels affected by mixing and averaged over the entire simulation time is shown in the top panel of Fig. 15. The white and gray lines denote the mean wind isotachs and the mean Q=0 line, respectively. The blue lines denote the mean tropopause calculated as for Fig. 14. All these lines are derived from the meteorological data averaged over the entire simulation time of 108 days.

Thus, a stronger STJ in the Northern Hemisphere is associated with a higher mixing intensity both below the jet and on its tropical side. Remarkably, the whole TTL, i.e. the region confined by the jets and θ-values between 350 and 420 K, is affected by mixing even if the largest contribution can be found on the tropical side of the STJs. Note that convection in the tropics below ≈340 K is described in CLaMS as an advective part of transport (i.e. in terms of trajectories and without mixing) and, consequently, does not significantly contribute to CLaMS mixing.

It should be emphasized that our concept of mixing-driven transport, in particular in the vicinity of the jets, does agree with the general understanding of STJ as seasonally-dependent barriers for isentropic transport (Haynes and Shuckburgh, 2000). This effect, which hinders horizontal transport of constituents from or into the TTL, is manifested in steep isentropic gradients of tracers perpendicular to the jet axis which form on a time scale of several weeks. This property can be seen in the meridional distribution of BT shown in the bottom right panel in Fig. 14 with a more permeable summer southern STJ in comparison to the northern STJ.

Although the highest mixing intensity in CLaMS is found on the tropical side of the winter STJ (see top panel of Fig. 15), such a jet, mainly due to a strong zonal orientation, serves as a very effective barrier for the isentropic transport. Conversely, a weak meandering summer STJ constitutes only a weak barrier for horizontal transport despite smaller mixing rates diagnosed in its vicinity. Thus, mixing through the barrier weakening the isentropic tracer gradients across the barrier does not necessarily follow the high local mixing rates diagnosed on both sides of the barrier.

One has to distinguish two different features of transport: the net transport across the barrier occurring on a time scale of several weeks and the local mixing rates on both sides of such a barrier occurring on a time scale of hours and homogenizing the tracer distributions separated by the barrier. Here, these two features are anti-correlated. On summary, the seasonal variability of the vertical mixing and horizonal permeability along and across the STJs are marked by black arrows in in the bottom right panel of Fig. 14 and in Fig. 15.

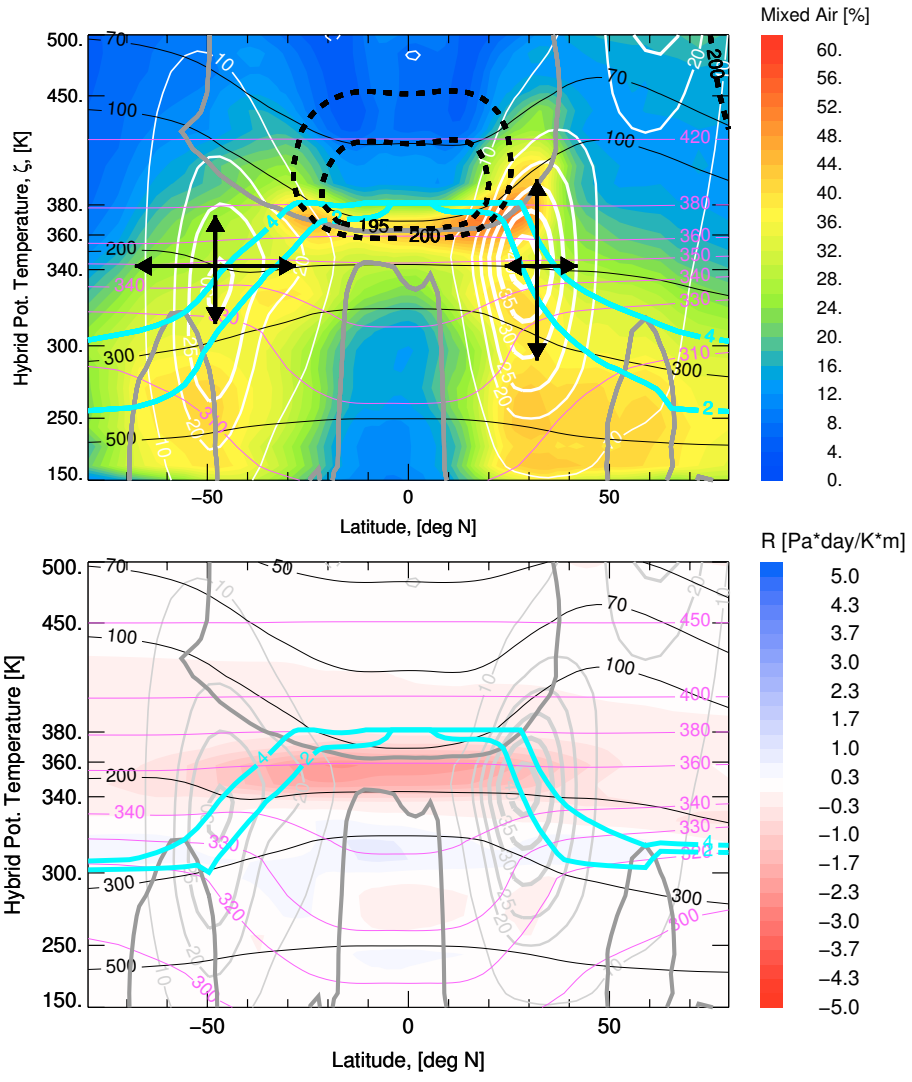

Fig. 15. Mean mixing intensity plotted as the percentage of air parcels affected by mixing (top) and the mean residual of the continuity equation R calculated in ζ-coordinates (bottom) and zonally averaged over the entire simulation time (108 days). The isotachs of the wind (top: white, bottom: light gray), the Q=0 line (dark gray) and the lowest temperature isolines (dashed black) are also shown. The blue lines approximate the tropopause.

Furthermore, even if the lowest mean temperatures (thick dashed black lines in Fig. 15) are symmetrically located over the equator, their position with respect to the jets is strongly asymmetric. Thus, despite a stronger vertical mixing at the tropical side of the Northern Hemisphere STJ, water vapor can be more effectively condensed above this region than during the upward transport occurring in the vicinity of the Southern Hemisphere STJ. This means that sufficiently strong convection interacting with the summer STJ could be a favored path for an effective upward transport of water vapor.

7 Discussion

Motivated by our simulations and comparison with the experimental data, we critically discuss now the main hypothesis of this paper stating that mixing, in particular the mixing scheme implemented in CLaMS, can effectively transport trace gases across the TTL and, consequently, has the potential to close the gap between the main convective outflow and the radiation-driven upward transport in the tropical stratosphere. We start our discussion with the analysis of the vertical velocity $\dot{\zeta}$ quantifying the advective part of transport and with the analysis of the interaction of $\dot{\zeta}$ with CLaMS mixing describing the diffusive part of transport.

To some extent the enhanced mixing in CLaMS around θ=380 K results from the necessity of filling the "white" regions in the left top panel of Fig. 14 with new air parcels (note that additional interpolations mean adding new air parcels which lead to additional mixing in the model (Konopka et al., 2004)). This can be understood as a consequence of the violation of the continuity equation caused by the use of hybrid vertical velocities where approximately above 300 hPa the ECMWF vertical p-velocities (which, by construction, fulfill the continuity equation) are gradually replaced by the vertical velocities calculated independently from a radiation scheme.

Because in the parts of the UT/LS region which are not affected by convection, the vertical velocities are, at least, two orders of magnitude smaller than the horizontal wind, their values derived from the continuity equation are strongly affected by the limited accuracy of the horizontal wind. Typical horizontal and vertical velocities in the UT/LS region are of the order of 10 and less than 0.01 m/s, respectively. Thus, horizontal wind accuracy higher than 0.1% would be necessary to resolve such small vertical winds.

This is the reason why most of the stratospheric CTMs like SLIMCAT (Feng et al., 2005) or CLaMS or trajectory-based studies in the stratosphere (Schoeberl and Newman, 1995; Rex et al., 1998) utilize vertical velocities calculated from a radiation scheme and why these velocities in the UT/LS region, if derived from the horizontal wind via the continuity equation, are used only in a statistical sense, e.g. in terms of monthly averaged values (Norton, 2002) or by appropriate climatologies of trajectories (Stohl, 2000; Fueglistaler et al., 2004).

In the bottom panel of Fig. 15, the mean residual R of the continuity equation in the ζ-coordinates (i.e. defined as the deviation of the continuity equation from zero) averaged over the simulated period is shown (see Holton, 1992, Eq. (4.31) with $\sigma = -g^{-1}\partial p/\partial\zeta$, σ-mass density in ζ coordinates). High absolute values of R identify regions where the velocity field does not fulfill the continuity equation. In particular, strong negative values of R as diagnosed in the TTL region (Fig. 15) are caused by too weak upwelling or too strong poleward transport. This can also be deduced from the transport at θ=360 K (not shown), where the air parcels slowly move away from the tropics, polewards, even if $\dot{\theta}\approx 0$ is valid at this surface.

A correction of the horizontal winds that does restore the validity of the continuum equation (and closes the white gaps in the left top panel of Fig. 14) can be achieved (B. Legras, personal communication), but such a correction is very small in comparison with the real horizontal winds and would not produce additional vertical transport across the TTL (in a CLaMS configuration without mixing). Furthermore, the intensity of the deformation-induced CLaMS mixing would not significantly change if these white gaps were filled with air parcels because the number of air parcels necessary to close these gaps is only a very small fraction (≈5%) of all the mixing events induced by the flow deformations (not shown).

Furthermore, sensitivity studies with respect to the impact of the choice of p_r (critical pressure level, below p_r=100 hPa we gradually replace the radiation-driven transport in the stratosphere by the ECMWF vertical velocities) show that by shifting p_r to higher values (p_r=300 hPa), we suppress the effect of convection and, in this way, we increase the gap between the main convective outflow and the stratosphere. On the other hand, by shifting p_r to lower values (p_r=10 hPa), the vertical transport across the TTL can occur without mixing (i.e. in terms of pure trajectory calculation) due to a decreasing residual error R in the continuity equation.

Comparison with the experimental data in the way discussed in previous sections show for all three choices of p_r that simulations with mixing describe much better the experimental data than the corresponding distributions calculated without mixing. This sensitivity study also indicates that, at least in the model, diffusive rather than advective transport (that is approximately equal zero) dominates the vertical distribution of species in the TTL. Furthermore, the ozone distributions calculated with CLaMS along the Geophysica flight tracks clearly overestimate and slightly underestimate the observations for p_r=300 and 10 hPa, respectively (i.e. the tropospheric influence is too weak for p_r=300 hPa and slightly too strong for p_r=10 hPa). Thus the preferred choice is p_r=100 hPa.

The question that still arises is, what is the mechanism that pushes the air parcels across the TTL if only 3-D ECMWF velocities (which are mass-conserving by construction) are used (as done e.g. by Fueglistaler et al., 2004). Considering our previous discussion, we think that probably slightly too high meridional, poleward velocities "pump", via the vertical velocities derived from the continuity equation, the air parcels upwards across the TTL. This can be a consequence of a bias in the assimilation system near the tropical tropopause but other explanations are also possible. On the other hand, the advective upward transport can occur at the same places where the diffusive transport diagnosed by CLaMS but we can also expect some differences. These differences, if present, would help to find out which transport mechanism is correct. We will analyze this point in the future.

Consequently, the diffusive fluxes in CLaMS have the potential to transport trace gases across the tropopause even if the advective fluxes point in opposite direction (see Appendix). Such a diffusive transport can be expected either isentropically across the STJs into the lowermost stratosphere or vertically into the stratosphere across the TTL, preferably along the STJs. It should be emphasized that the real physical mixing occurs on much smaller scales than the scales resolved by CLaMS (and most other global models, if not all) and is (probably) caused by such events like breaking

gravity or Kelvin waves or some other sources of instabilities which occur in the atmosphere.

In our approach, we follow the idea that such unresolved processes are driven by deformations in the large-scale flow (shear and strain). This idea that was first postulated by Smagorinsky (1963) couples mixing (that occurs on spatially unresolved scales) with gradients of the large-scale flow $D \sim \nabla \mathbf{u}$. In contrast to Eulerian models where (numerical) mixing in the form of numerical diffusion is proportional to the flow velocity, i.e. $D \sim \mathbf{u}$ (Courant et al., 1928), the CLaMS parameterization of mixing is nothing else but the Lagrangian realization of the $D \sim \nabla \mathbf{u}$ assumption.

To summarize, there are several options for reevaluating the transport processes in the TTL: either the mean convective outflow described in terms of the ECMWF large-scale vertical velocities is higher than 350 K and has to be parameterized by including sub-grid convection as discussed, for example in Tiedtke (1989), or the clear sky radiation has to be extended by accounting for the effect of thin cirrus clouds in the way proposed by Corti et al. (2006), or the hypothesis of the mixing-driven transport as proposed in this paper is, at least, a mechanism that effectively contributes to the lifting of the trace gases across the TTL.

8 Conclusions

The mixing-driven transport from the mean convective outflow across the TTL up into the stratosphere offers an alternative path for the troposphere-to-stratosphere transport (TST). Both the measurements on board the high altitude research aircraft Geophysica (ozone, water vapor, NO, NO_y, CH_4 and CO) in the altitude range spanning the TTL regions and the CLaMS studies with and without mixing support this idea in the sense that the model with mixing parameterization produces more realistic tracer distributions compared with the model configuration without mixing. The mixing-induced transport simulated with CLaMS occurs preferentially in regions with high vertical shear mainly found in the vicinity of the subtropical jets and, to some extent, in the outflow of the large-scale convection. Even when a strong winter subtropical jet acts as an effective barrier for isentropic transport, enhanced vertical transport can occur within its tropical flanks. Conversely, a weak summer jet can be characterized by a higher isentropic permeability and a weaker vertical transport. TST seems to be most effective if the outflow of mesoscale convective systems reaches the region penetrated by the subtropical jet.

Appendix A

Mass transport versus tracer transport

In order to understand differences between the transport of (passive) trace gases and that of the background atmosphere, let us consider m tracers with number densities n_i and volume mixing ratios μ_i given as $n_i = \mu_i n$, $i = 0, ..., m$ where $n = n_0$ ($\mu_0 = 1$) denotes the total number density of all molecules. Generally, one expects that on a sufficiently small but still macroscopic scale (i.e. containing a sufficiently large number of molecules) where diffusion processes can be neglected, the continuum equation describing the conservation of the number densities n_i is given by

$$\partial_t n_i + \nabla \cdot (n_i \mathbf{u}) = 0, \qquad i = 0, ..., m \tag{A1}$$

where $\mathbf{u}$ denotes the flow velocity on the spatial scale considered. Separating $\mathbf{u}$ into its mean part $\bar{\mathbf{u}}$, e.g. the ECMWF velocity fields valid on the spatial resolution of the model of about 100 km, and the fluctuation part $\mathbf{u}'$ describing the unresolved subgrid processes such as gravity waves, Eq. (A1) can be rewritten as (i.e. following the Raynolds averaging procedure):

$$\partial_t n_i + \nabla \cdot (n_i \bar{\mathbf{u}} + n_i \mathbf{u}') = 0. \tag{A2}$$

Thus, the total flux $\mathbf{j} = n_i \bar{\mathbf{u}} + n_i \mathbf{u}'$ consists of the mean flux $\bar{\mathbf{u}} = n_i \bar{\mathbf{u}}$ and of the additional flux, $\mathbf{j}'_i = n_i \mathbf{u}'$. The latter can be interpreted as a turbulent mass transport that can be parameterized by Fick's law, $\mathbf{j}'_i = n D \nabla \mu_i$ (D-diffusivity, see, e.g. Hall and Plumb (1994)). Consequently, the transport of all species can be described by

$$\partial_t (n \mu_i) + \nabla \cdot (n \mu_i \bar{\mathbf{u}} + n D \nabla \mu_i) = 0, \quad i = 0, ..., m. \tag{A3}$$

In particular, the transport of all air molecules n reduces with $i = 0$ and $\nabla \mu_0 = 0$ to

$$\partial_t n + \nabla \cdot (n \bar{\mathbf{u}}) = 0 \tag{A4}$$

Thus, the diffusive fluxes can change the tracer distributions n_i, without any change of the total number density n of all air molecules. Furthermore, it can occur that the diffusive flux of a tracer i, $n_i \bar{\mathbf{u}}'$, has the opposite direction and a higher absolute value than the advective flux $n_i \bar{\mathbf{u}}$.

This is, for example, the case within the TTL above the main convective outflow around $\theta = 350$ K and below the $Q = 0$ level around 360 K where, as discussed in this paper, the upward transport driven by vertical mixing can outweigh the large-scale, radiation-dominated, advective downward transport.

Acknowledgements. TROCCINOX was partially funded by the Commission of the European Community under contract EVK2-CT-2001-00122. The field experiment was performed with the Brazilian partner project TROCCIBAS, coordinated by IPMET (Insituto de Pesquisas Meteorologicas), Bauru, Sao Paulo, Brazil. The European Centre for Medium-Range Weather Forecasts (ECMWF) is acknowledged for meteorological data support. Excellent programming support was provided by N. Thomas. We are grateful for the contributions of D. Brunner and C. Schwierz providing us with the LAGRANTO trajectories. The authors wish to express their gratitude to the crew of the Geophysica, to all

the technicians and co-workers who contributed to the successful execution of the campaign and, in particular, to U. Schumann the coordinator of TROCCINOX. Finally, we thank four anonymous reviewers for their very constructive remarks.

Edited by: R. MacKenzie

References

Andrews, A. E., Boering, K. A., Daube, B. C., Wofsy, S. C., Hintsa, E. J., Weinstock, E. M., and Bui, T. B.: Empirical age spectra for the lower tropical stratosphere from in situ observations of CO_2: Implications for stratospheric transport, J. Geophys. Res., 104, 26 581–26 595, 1999.

Atticks, M. G. and Robinson, G. D.: Some features of the structure of the tropical tropopause, Quart. J. Roy. Meteorol. Soc., 109, 295–308, 1983.

Bradshaw, N. G., Vaughan, G., and Ancellet, G.: Generation of layering in the lower stratosphere by a breaking Rossby wave, J. Geophys. Res., 107(D2), 4011, doi:10.1029/2001JD000432, 2002a.

Bradshaw, N. G., Vaughan, G., Busen, R., Garcelon, S., Jones, R., Gardiner, T., and Hacker, J.: Tracer filamentation generated by small-scale Rossby wave breaking in the lower stratosphere, J. Geophys. Res., 107(D23), 4689, doi:10.1029/2002JD002086, 2002b.

Corti, F., Luo, B. P., Fu, Q., Vömel, H., and Peter, T.: The impact of cirrus clouds on tropical troposphere-to-stratosphere transport, Atmos. Chem. Phys., 6, 2539–2547, 2006, http://www.atmos-chem-phys.net/6/2539/2006/.

Courant, R., Friedrichs, K., and Lewy, H.: Über die partiellen Differenzengleichungen der mathematischen Physik, Mathematische Annalen, 100, 32–74, 1928.

Dethof, A., O'Neill, A., Slingo, J. M., and Smit, H. G. J.: A mechanism for moistening the lower stratosphere involving the Asian summer monsoon, Quart. J. Roy. Meteorol. Soc., 556(125), 1079–1106, 1999.

Doherty, G. M., Newell, R. E., and Danielsen, E. F.: Radiative heating rates near the stratospheric fountain, J. Geophys. Res., 89, 1380–1384, 1984.

Ehhalt, D. H., Rohrer, F., Schauffler, S., and Prather, M.: On the decay of stratospheric pollutants: Diagnosing the longest-lived eigenmode, J. Geophys. Res., 109(D08102), 347–350, doi:10.1029/2003JD004029, 2004.

Emanuel, K.: Tropical cyclons, Ann. Rev. Earth Planet Sci, 3, 75–104, 2003.

Feng, W., Chipperfield, M. P., Davies, S., Sen, B., Toon, G., Blavier, J. F., Webster, C. R., Volk, C. M., Ulanovsky, A., Ravegnani, F., von der Gathen, P., Jost, H., Richard, E. C., and Claude, H.: Three-dimensional model study of the Arctic ozone loss in 2002/2003 and comparison with 1999/2000 and 2003/2004, Atmos. Chem. Phys., 5, 139–152, 2005, http://www.atmos-chem-phys.net/5/139/2005/.

Folkins, I. and Martin, R. V.: The vertical structure of tropical convection and its impact on the budget of water vapor and ozone, J. Atmos. Chem., 62, 1560–1573, 2005.

Fueglistaler, S., Wernli, H., and Peter, T.: Tropical troposphere-to-stratosphere transport inferred from trajectory calculations, J. Geophys. Res., 109, D03108, doi:10.1029/2003JD004069, 2004.

Gettelman, A. and de Forster, P. M.: Definition and climatology of the tropical tropopause layer, J. Meteorol. Soc. Japan, 80(4B), 911–924, 2002.

Gettelman, A., Salby, M. L., and Sassi, F.: Distribution and influence of convection in the tropical tropopause region, J. Geophys. Res., 107(D10), 4080, doi:10.1029/2001JD001048, 2002.

Gettelman, A., de F. Fujiwara, P. M., Fu, Q., Voemel, H., Gohar, L. K., Johanson, C., and Ammeraman, M.: Radiation balance of the tropical tropopause layer, J. Geophys. Res., 109, D07103, doi:10.1029/2003JD004190, 2004.

Grooß, J.-U. and Müller, R.: Simulation of ozone loss in the Arctic winter 2004/05, Geophys. Res. Lett., 34, L05804, doi:10.1029/2006GL028901, 2007.

Grooß, J.-U., Günther, G., Müller, R., Konopka, P., Bausch, S., Schlager, H., Voigt, C., Volk, C. M., and Toon, G. C.: Simulation of denitrification and ozone loss for the Arctic winter 2002/2003, Atmos. Chem. Phys., 5, 2973–2988, 2005, http://www.atmos-chem-phys.net/5/2973/2005/.

Hall, T. M. and Plumb, R. A.: Age as a diagnostic of stratospheric transport, J. Geophys. Res., 99(D1), 1059–1070, 1994.

Haynes, P. and Anglade, J.: The vertical scale cascade in atmospheric tracers due to large-scale differential advection, J. Atmos. Sci., 54, 1121–1136, 1997.

Haynes, P. and Shuckburgh, E.: Effective diffusivity as a diagnostic of atmospheric transport, 2, Troposphere and lower stratosphere, J. Geophys. Res., 105, 22 795–22 810, 2000.

Hegglin, M. I., Brunner, D., Wernli, H., Schwierz, C., Martius, O., Hoor, P., Fischer, H., Spelten, N., Schiller, C., Krebsbach, M., Parchatka, U., Weers, U., Staehelin, J., and Peter, T.: Tracing troposphere-to-stratosphere transport above a mid-latitude deep convective system, Atmos. Chem. Phys., 4, 169–206, 2004, http://www.atmos-chem-phys.net/4/169/2004/.

Holton, J. R.: An Introduction to Dynamic Meteorology, Academic Press, London, 1992.

Holton, J. R., Haynes, P., McIntyre, M. E., Douglass, A. R., Rood, R. B., and Pfister, L.: Stratosphere-troposphere exchange, Rev. Geophys., 33, 403–439, 1995.

Kelly, K., Profitt, M. H., Chan, K. R., Loewenstein, M., Podolske, J. R., Strahan, S. E., Wilson, J. C., and Kley, D.: Water vapor and cloud water measurements over Darwin during the STEP 1987 tropical mission, J. Geophys. Res., 98, 8713–8723, 1993.

Konopka, P., Grooß, J. U., Günther, G., McKenna, D. S., Müller, R., Elkins, J. W., Fahey, D., and Popp, P.: Weak impact of mixing on chlorine deactivation during SOLVE/THESEO2000: Lagrangian modeling (CLaMS) versus ER-2 in situ observations., J. Geophys. Res., 108, 8324, doi:10.1029/2001JD000876, 2003.

Konopka, P., Steinhorst, H.-M., Grooß, J.-U., Günther, G., Müller, R., Elkins, J. W., Jost, H.-J., Richard, E., Schmidt, U., Toon, G., and McKenna, D. S.: Mixing and Ozone Loss in the 1999–2000 Arctic Vortex: Simulations with the 3-dimensional Chemical Lagrangian Model of the Stratosphere (CLaMS), J. Geophys. Res., 109, D02315, doi:10.1029/2003JD003792, 2004.

Konopka, P., Günther, G., McKenna, D. S., Müller, R., Offermann, D., Spang, R., and Riese, M.: How homogeneous and isotropic is stratospheric mixing? Comparison of CRISTA-1 observations with transport studies based on the Chemical Lagrangian Model of the Stratosphere (CLaMS), Quart. J. Roy. Meteorol. Soc.,

131(606), 565–579, doi:10.1256/qj.04.47, 2005.

Legras, B., Pisso, I., Berthet, G., and Lefevre, F.: Variability of the Lagrangian turbulent diffusion in the lower stratosphere, Atmos. Chem. Phys., 5, 1605–1622, 2005, http://www.atmos-chem-phys.net/5/1605/2005/.

Levine, J. G., Braesicke, P., Harris, N. R. P., Savage, N. S., and Pyle, J. A.: Pathways and timescales for troposphere-to-stratosphere transport via the tropical layer and their relevance for very short-lived substances, J. Geophys. Res., 112, D04308, doi:10.1029/2005JD006940, 2007.

Mahowald, N. M., Plumb, R. A., Rasch, P. J., del Corral, J., and Sassi, F.: Stratospheric transport in a three-dimensional isentropic coordinate model, J. Geophys. Res., 107(D15), 4254, doi:10.1029/2001JD001313, 2002.

McKenna, D. S., Konopka, P., Grooß, J.-U., Günther, G., Müller, R., Spang, R., Offermann, D., and Orsolini, Y.: A new Chemical Lagrangian Model of the Stratosphere (CLaMS): Part I Formulation of advection and mixing, J. Geophys. Res., 107(D16), 4309, doi:10.1029/2000JD000114, 2002.

Morcrette, J.-J.: Radiation and Cloud Radiative Properties in the European Centre for Medium-Range Weather Forecasts Forecasting System, J. Geophys. Res., 96(D5), 9121–9132, 1991.

Norton, W. A.: Longwave heating of the tropical lower stratosphere, Geophys. Res. Lett., 28(19), 3653–3656, doi:10.1029/2001GL013379, 2002.

Pan, L. L., Konopka, P., and Browell, E. V.: Observations and Model Simulations of Mixing near the Extratropical Tropopause, J. Geophys. Res., 111, D05106, doi:10.1029/2005JD006480, 2006.

Patmore, N. and Toumi, R.: An entropy-based measure of mixing at the tropopause, Quart. J. Roy. Meteorol. Soc., 132, 1949–1967, doi:10.1256/qj.05.84, 2006.

Pavelin, E. and Whiteway, J. A.: Gravity wave interactions around the jet stream, Geophys. Res. Lett., 29(21), 2024, doi:10.1029/2002GL015783, 2002.

Randel, W. and Park, M.: Deep convective influence on the Asian summer monsoon anticyclone and associated tracer variability observed with Atmospheric Infrared Sounder (AIRS), J. Geophys. Res., 111, D12314, doi:10.1029/2005JD006490, 2006.

Ren, C., MacKenzie, A. R., and Schiller, C.: Diagnosis of processes controlling water vapour in the tropical tropopause layer by a Lagrangian cirrus model, Atmos. Chem. Phys. Discuss., 7, 5515–5552, 2007, http://www.atmos-chem-phys-discuss.net/7/5515/2007/.

Rex, M., von der Gathen, P., Harris, N. R. P., Lucic, D., Knudsen, B. M., Braathen, G. O., Reid, S. J., De Backer, H., Claude, H., Fabian, R., Fast, H., Gil, M., Kyrö, E., Mikkelsen, I. S., Rummukainen, M., Smit, H. G., Stähelin, J., Varotsos, C., and Zaitcev, I.: In situ measurements of stratospheric ozone depletion rates in the Arctic winter 1991/92: A Lagrangian approach, J. Geophys. Res., 103, 5843–5853, 1998.

Schoeberl, M. R. and Newman, P. A.: A multiple-level trajectory analysis of vortex filaments, J. Geophys. Res., 100, 25 801–25 815, 1995.

Schumann, U., Huntrieser, H., Schlager, H., Höller, H., Bugliaro, L., and Gatzen, C.: Results from experiments over Europe and the continental tropics, in: Proceedings DACH-Meteorologentagung, Karlsruhe, pp. 1–10, 2004.

Sherwood, S. C. and Dessler, A. E.: A model for transport across the tropical tropopause, J. Atmos. Sci., 58, 765–779, 2001.

Simmons, A. J., Untch, A., Jakob, C., Kållberg, P., and Unden, P.: Stratospheric water vapour and tropical tropopause temperatures in ECMWF analyses and multi-year simulations, Quart. J. Roy. Meteorol. Soc., 125, 353–386, 1999.

Smagorinsky, J.: General circulation experiments with the primitive equations: I. The basic experiment, Mon. Wea. Rev., 91, 99–164, 1963.

Stefanutti, L., McKenzie, A. R., Santacesaria, V., Adriani, A., Balestri, S., Borrmann, S., Khattatov, V., Mazzinghi, P., Mitev, V., Rudakov, V., Schiller, C., Toci, G., Volk, C. M., Yushkov, V., Flentje, H., Kiemle, C., Redaelli, G., Carslaw, K. S., Noone, K., and Peter, T.: The APE-THESEO Tropical Campaign: An Overview, J. Atmos. Chem., 48, 1–33, 2004.

Stohl, A.: A one-year Langrangian "climatology" of airstreams in the northern hemisphere troposphere and lowermost stratosphere, J. Geophys. Res., 106(D7), 7263–7280, 2000.

Stohl, A., Haimberger, L., Scheele, M., and Wernli, H.: An intercomparison of results from three trajectory models, Meteorol. Appl., 8, 127–135, 2001.

Tie, X., Zhang, R., Brasseur, G., Emmons, L., and Lei, W.: Effects of lightning on reactive nitrogen and nitrogen reservoir species in the troposphere, J. Geophys. Res., 106, 3167–3178, 2001.

Tie, X., Brasseur, G., and Lei, W.: Global NOx production by lightning, J. Atmos. Chem., 43, 61–74, 2002.

Tiedtke, M.: A comprehensive mass flux scheme for cumulus parameterization in large-scale models, Mon. Wea. Rev., 117, 1779–1800, 1989.

Voigt, C., Schlager, H., Luo, B., Dörnbrack, A., Roiger, A., Stock, P., Curtius, J., Vössing, H., Borrmann, S., Davies, S., Konopka, P., Schiller, C., Shur, G., and Peter, T.: Nitric acid trihydrate (NAT) formation at low NAT supersaturations, Atmos. Chem. Phys., 5, 1371–1380, 2005, http://www.atmos-chem-phys.net/5/1371/2005/.

Wernli, H. and Davies, H. C.: A Lagrangian-based analysis of extratropical cyclones I: The method and some applications, Quart. J. Roy. Meteorol. Soc., 123, 467–489, 1997.

Zhong, W. and Haigh, J. D.: Improved Broadband Emissivity Parameterization for Water Vapor Cooling Rate Calculations, J. Atmos. Sci., 52(1), 124–138, 1995.

Zhou, J. and Lau, K. M.: Does a Monsoon Climate Exist over South America?, J. Climate, 11, 1020–1040, 1998.